

JOHNSON  
GRANT  
IN-33-OR  
189695  
798.

OPTIMIZATION OF THE LITHIUM/THIONYL CHLORIDE BATTERY

A FINAL REPORT  
for  
NASA GRANT NAG 9-177  
For the period January 1, 1988 to December 31, 1988

submitted to

NASA Scientific & Technical Information Facility  
P.O. Box 8757  
Baltimore/Washington International Airport  
Maryland 21240

(NASA-CR-184761) OPTIMIZATION OF THE  
LITHIUM/THIONYL CHLORIDE BATTERY Final  
Report, 1 Jan. - 31 Dec. 1988 (Texas A&M  
Univ.) 79 p CSCL 10C

N89-16114

Unclas  
G3/33 0189695

prepared by

Ralph E. White  
Department of Chemical Engineering  
Texas A&M University  
College Station, Texas 77843-3122

January 1989

## FINAL REPORT

The objective of the work over the past year was to develop and use models of the lithium/thionyl chloride ( $\text{Li/SOCl}_2$ ) cell to

1. aid in understanding the physical phenomena occurring in the cell,
2. reduce time intensive and costly experimental work, and
3. expedite the finding of acceptable and safe, yet optimal, designs.

These objectives have been partially satisfied by parameter estimation work with a one-dimensional mathematical model, developed earlier, and the heat flow patterns obtained from a two-dimensional thermal model.

This final report describes the progress which has been made in modeling the lithium/thionyl chloride cell over the past year. The one-dimensional mathematical model for a lithium/thionyl chloride cell, developed earlier, was used in conjunction with a parameter estimation technique to show how useful cell parameters could be obtained from experimental data. A paper on this work has been submitted to the *Journal of the Electrochemical Society* for publication and can be found in appendix A. A simplified two-dimensional model for the spirally wound design of this battery was developed and used to investigate the heat flow within the cell. A paper describing this work has been accepted for publication in the *Journal of the Electrochemical Society* and is included in this report as appendix B.

## APPENDIX A

**Estimation of Electro-Kinetic Parameters of the  
Lithium/Thionyl Chloride Cell Using a Mathematical Model**

by

**T. I. Evans<sup>1</sup> and R. E. White<sup>\*\*</sup>**

**Department of Chemical Engineering**

**Texas A&M University**

**College Station, Texas 77843**

submitted as a technical paper

to the

Editor

**Journal of the Electrochemical Society**

**10 South Main Street**

**Pennington, New Jersey 08534**

**September, 1988**

**Key Words:** discharge, exchange current density, lithium/thionyl chloride cell, parameter estimation, transfer coefficient

---

**\*\* Electrochemical Society Active Member**

<sup>1</sup> Present address: E. I. DuPont de Nemours & Co., Marshall Laboratory, 3500 Grays Ferry Ave., Philadelphia, PA 19146

## ABSTRACT

A one-dimensional mathematical model for the lithium/thionyl chloride primary cell is used in conjunction with a parameter estimation technique in order to estimate the electro-kinetic parameters of this electrochemical system. The electro-kinetic parameters include the anodic transfer coefficient and exchange current density of the lithium oxidation,  $\alpha_{a,1}$  and  $i_{o,1,ref}$ , the cathodic transfer coefficient and the effective exchange current density of the thionyl chloride reduction,  $\alpha_{c,2}$  and  $a^0 i_{o,2,ref}$ , and a morphology parameter,  $\xi$ . The parameter estimation is performed on simulated data first in order to gain confidence in the method. Data, reported in the literature, for a high rate discharge of an experimental lithium/thionyl chloride cell is used for an analysis.

## INTRODUCTION

This work is part of an ongoing effort to characterize the lithium/thionyl chloride (Li/SOCl<sub>2</sub>) cell in order to better understand the physical system and improve its safety and performance. The Li/SOCl<sub>2</sub> cell is an attractive primary energy source because of its high energy density (1, 2). A description of the Li/SOCl<sub>2</sub> cell along with the safety hazards it exhibits is discussed elsewhere (2).

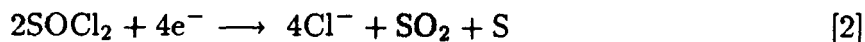
A detailed mathematical model of this battery has been presented (3). This model is used here in conjunction with a parameter estimation technique in order to establish a means to estimate the electro-kinetic parameters which aid in describing the physical system. The assumptions and governing equations used in the model are given elsewhere (3). A description of the model parameters, the sensitivity of the model predictions to changes in these parameters, and estimates of these parameters based on available experimental data (4) is presented next.

## MODEL PARAMETERS

The model (3) includes several reactions: the oxidation of lithium at the anode



the reduction of SOCl<sub>2</sub> at the cathode

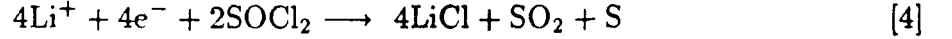


and the precipitation of LiCl on the pore surfaces of the cathode during discharge by the following reaction



Due to the low solubility of LiCl in the SOCl<sub>2</sub> + LiAlCl<sub>4</sub> mix (5), reaction [3] is assumed to occur completely and instantaneously. Thus, reactions [2] and [3] can be combined to

yield one overall reaction representing the processes occurring within the porous cathode  
(3)



Four species are included in the model,  $\text{Li}^+$ ,  $\text{AlCl}_4^-$ ,  $\text{SOCl}_2$ , and  $\text{LiCl}$ .

The electrochemical reaction rates,  $i_k$ , depend upon the local concentrations of the chemical species, the potential driving force for reaction, and temperature. Analogous to chemical kinetics, these dependencies are not described by fundamental laws. The Butler-Volmer polarization equation for a flat plate electrode (6, 7) is used in the model  
(3)

$$i_k = i_{o,k,ref} \left[ \prod_i \left( \frac{c_i}{c_{i,ref}} \right)^{p_{i,k}} \exp \left( \frac{\alpha_{a,k} F}{RT} \eta_k \right) - \prod_i \left( \frac{c_i}{c_{i,ref}} \right)^{q_{i,k}} \exp \left( -\frac{\alpha_{c,k} F}{RT} \eta_k \right) \right] \quad [5]$$

where

$$\eta_k = \Phi_s - \Phi_{o,e} - U_{k,ref} \quad [6]$$

In Eq. [6],  $\eta_k$  is the potential driving force for electrochemical reaction  $k$ . The electro-kinetic parameters  $i_{o,k,ref}$ ,  $\alpha_{a,k}$ , and  $\alpha_{c,k}$  are the exchange current density, anodic transfer coefficient, and cathodic transfer coefficient for reaction  $k$ , respectively. These electro-kinetic parameters characterize the electrochemical reaction via Eq. [5] and are the parameters that are sought in this work. Note that the transfer coefficients for a given reaction sum to the total number of electrons involved in that reaction

$$\alpha_{a,k} + \alpha_{c,k} = n_k \quad [7]$$

Hence, only one of the transfer coefficients need be estimated and the remaining one can be obtained from Eq. [7].

Equation [5] must be modified slightly in order to describe the rate of reaction [4] in the porous carbon cathode. The rate of reaction [4] must be expressed per unit volume of porous electrode. This change is accomplished by premultiplying Eq. [5] by the available active surface area per unit volume of electrode,  $a$ . The variable  $a$  changes as the LiCl precipitates on the pore walls, according to reaction [4], and can be described by (8, 9)

$$a = a^o \left[ 1 - \left( \frac{\epsilon^o - \epsilon}{\epsilon^o} \right)^\xi \right] \quad [8]$$

where  $\xi$  is an experimentally determined parameter used to describe the morphology of the precipitate. In writing Eq. [8] it is assumed that all the LiCl produced from reaction [4] precipitates instantaneously and passivates the surface it covers. Large values of  $\xi$  indicate needle-shaped deposits whereas small values represent flat deposits (9). Premultiplying Eq. [5] by Eq. [8] yields the following equation for the rate of reaction [4] per unit volume of porous electrode

$$j = a^o \left[ 1 - \left( \frac{\epsilon^o - \epsilon}{\epsilon^o} \right)^\xi \right] i_{o,4,ref} \left[ \prod_i \left( \frac{c_i}{c_{i,ref}} \right)^{p_{i,4}} \exp \left( \frac{\alpha_{a,k} F}{RT} \eta_4 \right) - \prod_i \left( \frac{c_i}{c_{i,ref}} \right)^{q_{i,4}} \exp \left( -\frac{\alpha_{c,k} F}{RT} \eta_4 \right) \right] \quad [9]$$

The effective exchange current density for reaction [4] is the product  $a^o i_{o,4,ref}$ . In all, nine electro-kinetic parameters,  $i_{o,1,ref}$ ,  $\alpha_{a,1}$ ,  $\alpha_{c,1}$ ,  $a^o i_{o,4,ref}$ ,  $\alpha_{a,4}$ ,  $\alpha_{c,4}$ ,  $q_{+,1}$ ,  $q_{+,4}$ , and  $q_{o,4}$ , and one morphology parameter,  $\xi$ , are used (3); two of the transfer coefficients,  $\alpha_{c,1}$  and  $\alpha_{a,4}$ , are not independent quantities because they can be calculated from  $\alpha_{a,1}$  and  $\alpha_{c,4}$  via Eq. [7].

Several parameters are used in the model (3) to describe the species transport. The diffusion coefficient,  $D$ , is used to characterize the diffusion of the salt ( $\text{LiAlCl}_4$ )

in the solvent ( $\text{SOCl}_2$ ) due to concentration gradients in the cell. In the model (3), the diffusion coefficient is calculated using the following expression

$$D = \beta_6 \exp(\beta_5/T) \quad [10]$$

where  $\beta_5$  and  $\beta_6$  are constants. The transference number of charged species  $i$ ,  $t_i^\square$ , is used to describe the migration of species  $i$  in the cell due to the electric field. Two charged species are considered in the model,  $\text{Li}^+$  and  $\text{AlCl}_4^-$ , therefore two transference numbers are used,  $t_+^\square$  and  $t_-^\square$ . Only one transference number is independent because they must sum to one

$$t_+^\square + t_-^\square = 1 \quad [11]$$

When no concentration gradients exist, the transference number of a particular species represents the fraction of the current carried by that species (10). When concentration gradients do exist, however, the transference number loses this physical interpretation but can be thought of as a weighting factor which determines the importance of the migration term in the flux expression.

In order to use the model (3) to predict cell performance for various cell designs, investigate scale-up, and optimize a  $\text{Li}/\text{SOCl}_2$  cell, estimates of the electro-kinetic parameters are needed. Given experimental data for a particular  $\text{Li}/\text{SOCl}_2$  cell or half-cell, along with the complete cell specifications, it should be possible to use a parameter estimation technique to obtain these electro-kinetic parameters. A sensitivity analysis is conducted first to determine the relative importance of each parameter, followed by parameter estimation using simulated data to gain confidence in the procedure, and finally an experimental discharge curve is used to find the  $\text{SOCl}_2$  electro-kinetic parameters.

## SENSITIVITY ANALYSIS

It is important to determine the sensitivity of the model predictions to changes in the electro-kinetic parameters. If the model predictions are relatively insensitive to one or more of the parameters then a fairly wide range of values for these insensitive parameters could be used without significantly affecting the predictions of the model. Such parameters need to be identified so that they can be discarded from the parameter estimation procedure. Also, it is often the case that the more parameters that are estimated, the more uncertain are the estimates due to interaction between the parameters, poor scaling, and round-off error (11). In addition to the identification of insensitive parameters, the operating conditions or situations under which the sensitivity to given parameters is maximum can be determined.

The sensitivity of the model predictions to changes in parameters is determined here by monitoring the change in cell voltage. While holding all other parameters constant, the parameter of interest is perturbed slightly and the resulting change in cell voltage is noted. A sensitivity coefficient is calculated as follows

$$SC_i = \frac{\sum_{j=1}^n |\Delta E(t_j)|}{m |\Delta P_i|} \quad [12]$$

where

$$\Delta E(t_j) = E(t_j) - E^*(t_j) \quad [13]$$

$$\Delta P_i = \frac{P_i - P_i^*}{P_i^*} \quad [14]$$

$P_i$  and  $P_i^*$  are the perturbed value of electro-kinetic parameter  $i$  and the reference value of parameter  $i$ , respectively.  $E(t_j)$  is the value of the cell voltage at time  $t_j$  when using  $P_i$  and  $E^*(t_j)$  is the value of the cell voltage at time  $t_j$  when using  $P_i^*$ . In Eq. [12],  $n$  is the number of times over which the voltages are compared.

Many factors come into play when calculating the sensitivity coefficients. The influence of a particular parameter on cell voltage varies depending on the discharge rate, depth of discharge, and temperature. For example, the exchange current densities,

$i_{o,1,ref}$  and  $a^o i_{o,4,ref}$ , strongly influence the initial drop in cell voltage from the open-circuit potential (12). On the other hand, the powers on the concentration terms,  $q_{+,1}$ ,  $q_{+,4}$ , and  $q_{o,4}$ , have more influence later in the discharge when concentrations change more drastically due to localized reactant depletion. Therefore, the value of  $n$  in Eq. [12] is chosen so that approximately 80% of the discharge is included in the analysis.

The results of the sensitivity analysis are shown in Fig. 1 and 2. Figure 1 shows the sensitivity of the cell voltage to the electro-kinetic parameters describing the lithium oxidation, reaction [1], over a range of discharge rates. Figure 2 is an analogous plot for reaction [4]. The most influential parameter by far is the lithium oxidation transfer coefficient  $\alpha_{a,1}$ . This is to be expected because  $\alpha_{a,1}$  is in the exponential portion of Eq. [5]. The lithium oxidation exchange current density,  $i_{o,1,ref}$ , and  $\text{SOCl}_2$  reduction transfer coefficient are next followed by the effective  $\text{SOCl}_2$  exchange current density,  $a^o i_{o,4,ref}$ , and the morphology parameter,  $\xi$ . The electro-kinetic parameters describing the  $\text{SOCl}_2$  reduction display less influence than those describing the lithium oxidation. This could be due to the fact that the lithium oxidation occurs at the surface of a flat-plate electrode (a boundary condition in the model) whereas the  $\text{SOCl}_2$  reduction occurs throughout the porous structure of the cathode (a pseudohomogeneous region in the model). The overall influence of the  $\text{SOCl}_2$  reduction electro-kinetic parameters is, in affect, decreased because the change in voltage is distributed over the thickness of the cathode as opposed to the change occurring all at one point. The exponents on the power terms,  $q_{+,1}$ ,  $q_{+,4}$ , and  $q_{o,4}$  show little influence at the discharge rates investigated. They are discarded from most of the parameter estimation work presented next; they are set to the corresponding stoichiometric value as is often done.

The sensitivity of model predictions to changes in two of the transport parameters,  $t_i^+$  and  $\beta_6$ , was briefly investigated as shown in Fig. 3. At high current densities, the transference number shows substantial influence and the effects of diffusion become

important. However, the sensitivity to these parameters is reduced as the current is reduced because the electrochemical reaction rates become controlling. This result suggests that a parameter estimation procedure aimed at finding the electro-kinetic parameters should be performed with low-rate data so that species transport will not interfere with the accuracy of the estimates.

## PARAMETER ESTIMATION

Klinedinst and Domeniconi (4) investigated the performance of a single Li/SOCl<sub>2</sub> cell with various carbon electrode thicknesses and operated over various discharge rates. Their experimental test cell has some features which make it attractive for obtaining experimental cell voltages for comparison with the model predictions here. The single cell, corresponding to the single cell model (3), is immersed in excess electrolyte and hence the cell temperature remains nearly constant throughout the discharge. The electrolyte is introduced into the test cell shortly before the beginning of the test (approximately 10 minutes before) suggesting that little or no secondary LiCl film is present on the Li electrode. Also, the anode, separator, and cathode are pressed together with a weight so that no reservoir exists between the separator and cathode.

The cell model (3) was changed to simulate this test cell for the parameter estimation. The film and reservoir regions were eliminated from the model by setting the film porosity equal to the separator porosity, removing the reservoir calculations from the model, and modifying slightly the boundary conditions at the reservoir/porous electrode interface to be those for the separator/porous electrode interface. The model inputs for simulating the test cell of Klinedinst and Domeniconi are listed in Table I.

Initially, simulated data for both a 1 mA/cm<sup>2</sup> and a 31 mA/cm<sup>2</sup> discharge were used for the parameter estimation in order to gain confidence in the procedure and guide

future experimentation. Experimental data, for a 31 mA/cm<sup>2</sup> discharge, were used to estimate the SOCl<sub>2</sub> reduction electro-kinetic parameters for this high-rate discharge.

*Reformulation of the Butler-Volmer Equation:*

To reduce the interaction between parameters in the least-squares procedure, it is sometimes necessary to reformulate the model equations. Parameter interaction is evident when small changes in the parameters produce similar changes in the objective function. Interaction often occurs when the parameters appear as a product somewhere in the governing equation. Interaction can be reduced if the equation is rewritten so that the parameters appear in separate terms.

As shown in Eq. [9], the electro-kinetic parameters in the Butler-Volmer equation appear in product terms as opposed to separate terms. The Butler-Volmer equation can be rearranged by first taking the natural logarithm and then taking the exponent of the various terms (12). For the parameter estimation used here, Eq. [9] is written as follows

$$j = \exp[f_1 + f_2] - \exp[f_1 + f_3 + f_4 + f_5] - \exp[f_1 + f_2 + f_6] + \exp[f_1 + f_3 + f_4 + f_5 + f_6] \quad [15]$$

where

$$f_1 = \ln(a^o i_{o,4,ref}) \quad [16]$$

$$f_2 = \frac{\alpha_{a,4} F}{RT} (\Phi_1 - \Phi_2 - U_{4,ref}) \quad [17]$$

$$f_3 = q_{+,4} \ln\left(\frac{c}{c_{ref}}\right) \quad [18]$$

$$f_4 = q_{o,4} \ln\left(\frac{c_o}{c_{o,ref}}\right) \quad [19]$$

$$f_5 = -\frac{\alpha_{c,4} F}{RT} (\Phi_1 - \Phi_2 - U_{4,ref}) \quad [20]$$

$$f_6 = \xi \ln\left(\frac{\epsilon^o - \epsilon}{\epsilon^o}\right) \quad [21]$$

Equation [5] for reaction [1] is rewritten in a similar fashion. As a result of this reformulation, the parameters used in the parameter estimation procedure are  $\ln(a^o i_{o,4,ref})$ ,  $\alpha_{c,4}$ ,  $\xi$ ,  $\alpha_{a,1}$ , and  $\ln(i_{o,1,ref})$ .

*Introduction of Noise into Simulated Data:*

In order to test the ability of the parameter estimation procedure to predict the model parameters within reasonable accuracy, random noise was added to the simulated data. A random number generator from the IMSL library [15] was used to generate a normally distributed number,  $\varphi$ , with mean zero and variance one (i.e.,  $\sim N(0,1)$ ). The noise was added to the predicted value of the cell potential at time  $t_j$ ,  $E(t_j)$ , as follows

$$E(t_j)_{\text{with noise}} = E(t_j) + \varphi Z \quad [22]$$

where  $Z$  is the average level of noise (in mV) presumably inherent in the measurement of the cell voltage. Three levels of  $Z$  were investigated here, 0.5 mV, 1 mV, and 2 mV. It is realistic to assume that the experimental measurements of the cell voltage would be accurate to within 2.0 mV.

*Calculation of Confidence Intervals for Parameter Estimates:*

An estimate of a parameter has little meaning unless it is accompanied by some approximation of the possible error it possesses. Here, confidence intervals for the parameter estimates can be estimated by using the following formula (14)

$$P_i = \hat{P}_i \pm t_{(1-\frac{\gamma}{2}),(n-m)} s_{P_i} \quad [23]$$

In Eq. [23],  $\hat{P}_i$  is the estimate of  $P_i$ ,  $t_{(1-\frac{\gamma}{2}),(n-m)}$  is the t-distribution at the  $(1-\frac{\gamma}{2}) \times 100$  percent confidence level,  $(n-m)$  is the degrees of freedom,  $n$  is the number of observations,  $m$  is the number of parameters estimated, and  $s_{P_i}$  is the estimate of the variance of  $P_i$  which is calculated from the sum of squares of the error,  $s_E^2$ , as follows:

$$s_{P_i} = \sqrt{C_{ii} s_E^2} \quad [24]$$

In Eq. [24],  $C_{ii}$  is an element of the matrix  $(\mathbf{J}^T \mathbf{J})^{-1}$  (i.e., inverse of the approximate Hessian, see appendix B in ref. 15). The estimate of the variance in the error,  $s_E^2$ , is calculated from the sum of squares of the residual errors ( $SSR$ ) as follows

$$s_E^2 = \frac{SSR}{n - m} = \frac{\sum_{j=1}^n (E(t_j)_{obs} - E(t_j)_{pred})^2}{n - m} \quad [25]$$

*Parameter Estimation Using High-Rate Simulated Data:*

The use of high-rate (e.g., 30 mA/cm<sup>2</sup>) discharge data for parameter estimation seems to offer several advantages. High rate discharges occur over a relatively small time as opposed to low rate discharges (e.g., about 1 hour for a 30 mA/cm<sup>2</sup> discharge as opposed to approximately 50 hours for a 1 mA/cm<sup>2</sup> discharge of a Li/SOCl<sub>2</sub> cell). This means less time in the lab and, perhaps, less computer time to simulate the discharge. Often, the shapes of voltage-time curves for high-rate discharges are much more curved than the relatively flat voltage-time curves for low-rate discharges thus offering more information for the parameter estimation.

Here, however, the use of high-rate data exhibited several disadvantages. First, the influence of species transport becomes important at the higher discharge rates. For example, at 100 mA/cm<sup>2</sup> the sensitivity coefficient, as calculated using Eq. [12], for the transference number is 0.3 which is second only to the sensitivity coefficient of  $\alpha_{a,4}$ , 0.53. Due to the uncertainty in the transference number and the lack of data for the diffusion coefficient (see appendix A in ref. 15) it is best to stay clear of those operating regions where species transport is a controlling aspect of the cell discharge. Secondly, at high rates much interaction exists between the electro-kinetic parameters. This interaction can be seen in Fig. 4 which is a plot of the time-dependent sensitivity coefficients (i.e., the elements of the Jacobian matrix, as shown in appendix B in ref. 15) for a 31 mA/cm<sup>2</sup> simulated discharge. These sensitivity coefficients are calculated using Eq.

[12] except that the perturbation in each parameter,  $\Delta P$ , is not scaled by  $P_i^*$  as in Eq. [14] but is calculated as follows

$$\Delta P_i = P_i - P_i^* \quad [26]$$

Note that three of the five parameters,  $\ln(a^o i_{o,4,ref})$ ,  $\alpha_{a,1}$ , and  $\ln(i_{o,1,ref})$ , influence the cell voltage in the same fashion. This similar influence (i.e., interaction) is shown by the three straight parallel lines (14) in the figure. Thus, only one of these three parameters can be determined independently. Note also that the two lithium oxidation parameters cannot be individually obtained at high rates.

Another indication of this interaction is the condition number of the approximate Hessian (11) (see appendix B in ref. 15). The condition number of a matrix is the ratio of its largest eigenvalue to its smallest eigenvalue. A matrix is called ill-conditioned when its condition number is large. The larger the condition number, the more substantial the change in the solution even with very small changes in the data. In essence, a large condition number here means that a unique set of electro-kinetic parameters is more difficult to find; many sets will reduce the objective function to nearly the same value. The condition number for the approximate Hessian here was on the order of  $1 \times 10^{18}$ . The reason for this ill-conditioning could be the fact that transport becomes more important at higher rates which serves to decrease the influence of changes in the electro-kinetic parameters on cell performance.

Though interaction between some of the parameters exists at high rates, several attractive features can be noted. If the lithium oxidation parameters,  $i_{o,1,ref}$  and  $\alpha_{a,1}$ , are known *a priori* via independent means, then the  $\text{SOCl}_2$  electro-kinetic parameters can be determined using high-rate data. This ability is shown in Table II where  $\ln(a^o i_{o,4,ref})$ ,  $\alpha_{c,4}$ , and  $\xi$  are estimated from simulated 31 mA/cm<sup>2</sup> data with 0.5 mV added random noise. This ability is important because the  $\text{SOCl}_2$  electro-kinetic parameters will probably change with discharge rate due to changes in the active surface

area in the porous electrode as discharge proceeds. In addition, the sensitivity of the predicted cell voltage to changes in  $\xi$  seems to be greater at high rates than at low rates thus enabling better estimates of  $\xi$ . This can be seen by comparing the sizes of the confidence intervals for  $\xi$  here with those in the next section.

*Parameter Estimation Using Low-Rate Simulated Data:*

Parameter estimation on low-rate data (e.g., 1 mA/cm<sup>2</sup>) remedies some of the problems encountered with the high-rate data. The interaction between parameters is decreased. Figure 5 is a plot of the sensitivity coefficients versus time for the 1 mA/cm<sup>2</sup> simulated discharge. The curves have differing slopes and shapes, as opposed to those for the high-rate case as shown in Fig. 4, indicating that the various parameters affect cell voltage differently and hence can be determined independently. Note that these coefficients are calculated using the known values of the electro-kinetic parameters. Table III lists the condition numbers for the approximate Hessians for various combinations of the parameters; the various combinations are indicated by case. The condition numbers for cases A and E are low suggesting that parameter estimations for either of these cases ought to be straightforward and the confidence intervals on the parameter estimates small (11). Here, the term straightforward parameter estimation means that the search proceeds to the solution given a variety of initial guesses that can be "far" from the correct solution. More difficult parameter estimation runs involve multiple initial guesses in order to make sure the estimates obtained with a particular initial guess are not those at a local minimum. A comparison of cases A and B shows that estimates for all three SOCl<sub>2</sub> electro-kinetic parameters will be more difficult to obtain than estimates for  $\ln(a^o i_{o,4,ref})$  and  $\alpha_{c,4}$  alone. Case G shows that the eight-parameter problem is extremely ill-conditioned, meaning much interaction between parameters and very large confidence intervals on the parameter estimates. Therefore,  $q_{+,1}$ ,  $q_{+,4}$ , and

$q_{0,4}$  are omitted from the following parameter estimation work and are set to their stoichiometric values as in Table II of ref. 3.

The simulated data for the  $1 \text{ mA/cm}^2$  discharge investigated here, with added noise, are shown in Fig. 6. The model inputs are listed in Table I. The data in Fig. 6 spans approximately 50% of the discharge. Although predicted discharge times are much longer for low-rate than for high-rate, the solution times for low-rate cases may actually be smaller than those for high-rate cases. Solution times depend upon the number of spatial nodes, the size of the time steps, and the number of iterations (at each time) to converge upon the solution. At low-rates, changes in the dependent variables (electrolyte concentration, current, and potential) in space and time occur much less rapidly than at high-rate. Therefore, fewer node points and larger time steps can be used at low-rate than at high-rate to maintain three-digit accuracy. For example, 81 nodes and a maximum time step of 37.5 seconds were used to maintain three-digit accuracy for the  $31 \text{ mA/cm}^2$  discharge results reported earlier. Here, for the  $1 \text{ mA/cm}^2$  discharge, 21 nodes and a maximum time step of 2000 seconds were sufficient. This result eliminates the advantage of using high-rate data to reduce solution time; the only disadvantage to using low-rate data is the length of time it takes to collect the experimental data.

The results of the parameter estimation runs are shown in Tables IV - VII. As expected, the runs for cases A and E were straightforward with narrow confidence intervals for the parameter estimates. As shown in Tables IV and V, the initial guesses are at different extremes and up to two orders of magnitude away from the true solution. Notice how the confidence intervals increase as the noise level increases which is to be expected. Case E may be useful when estimates of the  $\text{SOCl}_2$  electro-kinetic parameters have been obtained independently. Similarly, Case A may be needed when estimates of the lithium oxidation electro-kinetic parameters are available and an estimate of  $\xi$  is known from independent studies. Table VI lists parameter estimation runs for case B, all

three  $\text{SOCl}_2$  reduction electro-kinetic parameters. This case, as shown in the previous section, can be used to determine both low-rate and high-rate values of  $a^\circ i_{o,4,ref}$ ,  $\alpha_{c,4}$ , and  $\xi$  when estimates of  $\alpha_{a,1}$  and  $\ln(i_{o,1,ref})$  are known. Notice the increase in the size of the confidence intervals from Table V to Table VI. The estimation of the additional parameter,  $\xi$ , adds greater uncertainty to the parameter estimates, as expected. Also, judging from the large increase in condition number from case A to case B in Table III, some interaction between these parameters is evident.

Table VII lists parameter estimation runs for case D. The ability to estimate all five electro-kinetic parameters at once, as in case D, is attractive. Simultaneous estimation of all parameters in the model usually provides parameter estimates possessing superior predictive capability. Often, independently determined parameter estimates do not predict the behavior of the entire unit very well. For example, independent estimates of the lithium oxidation parameters and  $\text{SOCl}_2$  reduction parameters may not be useful for predicting the behavior of the  $\text{Li}/\text{SOCl}_2$  cell. These independent estimates might be obtained from rotating disk electrode experiments and a corresponding mathematical model. In Table VII, note that for the data with added 0.5 mV noise the confidence intervals on certain parameter estimates are unacceptably large. This uncertainty in the predictions is due to parameter interaction (note the relatively large condition number in Table III) even at this low rate of discharge. The five parameters can be obtained with no noise, as shown in Table VII, but it is unrealistic to expect exact measurements and the model to be an exact description of the physical system. It may be useful to obtain all five parameters simultaneously, even though the confidence intervals are large, because the estimates should still provide an excellent fit of the model predictions to the experimental data (notice the small SSR in Table VII). The parameter estimation runs for cases B and D were not straightforward. Certain initial guesses of the parameters detoured the search algorithm to local minimums. For example, for the case D runs,

the initial guesses of the exchange current densities needed to be within an order of magnitude and the transfer coefficient guesses needed to be within about half of their true value in order to reach convergence. The algorithm could not escape these local minimums within a reasonable number of iterations (e.g., 60 iterations).

An alternative to predicting all five parameters simultaneously would be to obtain estimates for some of the parameters independently (for example, the lithium oxidation parameters) and then use these estimates in the cell model to obtain the remaining parameters (the  $\text{SOCl}_2$  reduction parameters) using data from the entire cell. In addition, separate data for each electrode in the  $\text{Li}/\text{SOCl}_2$  cell can be obtained by constructing half-cells. For example, a lithium electrode half-cell could be constructed from a  $\text{Li}/\text{SOCl}_2$  cell by placing a reference electrode near the surface of the lithium electrode. The lithium electrode is the working electrode, a second lithium electrode (with high impedance) placed near the surface of the working electrode could act as the reference electrode, and the porous carbon cathode is the counter electrode. The potential of the lithium electrode, as it changes with time, could then be measured relative to the reference electrode. Predictions of the Li electrode potential could be obtained from a model of the working electrode / reference electrode system, consisting of equations presented earlier for the entire  $\text{Li}/\text{SOCl}_2$  cell. These predictions could then be compared with the experimental values to obtain estimates of the electro-kinetic parameters of the lithium electrode.

*Parameter Estimation Using Available Experimental Data:*

The analyses using simulated data in the previous sections have shown the need to collect low-rate data from a well defined experimental cell. Unfortunately, no such experimental data is currently available. Various experimental voltage-time curves have been reported (16, 17, 18, 19) but it is difficult to use this data due to the lack of cell specifications given (e.g., porous electrode porosity and thickness, initial electrolyte

concentration, temperatures, and separator porosity and thickness). In addition, large differences exist in the experimental data which can be attributed to the different electrode materials, initial electrolyte concentrations, operating conditions, and cell dimensions used.

Using data from Klinedinst (20), for a  $31 \text{ mA/cm}^2$  discharge of an experimental cell (4), estimates of the  $\text{SOCl}_2$  reduction electro-kinetic parameters were obtained. The lithium oxidation electro-kinetic parameters were arbitrarily set to the values listed in Table I of ref. 3. These values are well within ranges commonly used in the literature for electrochemical reactions. Initially, a by-hand trial and error search was conducted to find electro-kinetic parameters giving model predictions close to the experimental results. It was hoped that this search would provide initial guesses in the vicinity of their actual values to aid in the parameter estimation. Two sets of initial guesses were tried, as shown in Table VIII as Run # 1 and Run # 2, and the same final parameter values were obtained to within the confidence limits shown. The values are listed in Table VIII and the predicted voltage curve, obtained using the estimates from Run # 1, is superimposed on the experimental data in Fig. 7. Note that the confidence intervals for  $a^\circ i_{o,4,ref}$  and  $\xi$  in Run # 1 and Run # 2 are large relative to the estimated values of the parameters. To reduce the uncertainty in the estimate of  $a^\circ i_{o,4,ref}$ ,  $\xi$  was set to a value of 0.02 (a value between the estimates of  $\xi$  in Run # 1 and Run # 2) for Run # 3. This procedure (estimating all three  $\text{SOCl}_2$  electro-kinetic parameters, setting  $\xi$  to an average value, and then estimating  $a^\circ i_{o,4,ref}$  and  $\alpha_{c,4}$ ) gives estimates of  $a^\circ i_{o,4,ref}$  and  $\alpha_{c,4}$  with reasonable confidence intervals and an estimate of  $\xi$  in the vicinity of its best value.

Notice in Fig. 7 that the first experimental data point used occurs some time after the beginning of the discharge. This is due to the fact that the beginning behavior of experimental discharge curves are very different. Some exhibit a very sudden and

large initial decrease followed by a time of voltage recovery and is known as the voltage-delay phenomena. Others show a steady decrease, with an initial large decrease, as the model predictions do. The voltage-delay phenomena in Li/SOCl<sub>2</sub> cells has been studied by Dey (21) and has been associated with the LiCl film. Slow voltage recovery is associated with slow mechanical disruption of the film. The model does not account for this voltage-delay phenomena and therefore initial experimental data were excluded from the parameter estimation.

## CONCLUSIONS

The sensitivity analysis and parameter estimation performed here for the model presented by Evans *et al.* (3) yields several conclusions. The test cell of Klinedinst and Domeniconi (4) offers a constant temperature environment, a single cell (as opposed to a stack), elimination of film and reservoir regions, and well-defined thicknesses of the cell components. Low-rate data should be used to obtain estimates of the electrokinetic parameters so that interaction between parameters is small. Low rate data is just as efficient to use in the parameter estimation procedure as is high rate data because the number of nodes can be decreased and the time step increased so that the solution times are comparable. Also, at low rates the effects of species transport are minimal. Once estimates of the lithium oxidation parameters are available, the electrokinetic parameters describing the SOCl<sub>2</sub> reduction on the porous carbon electrode can be determined even for high discharge rates. These parameters will change with electrolyte composition, type of carbon used for the electrode, and temperature.

## NOMENCLATURE

$a$	specific electroactive surface area of the porous electrode, $\text{m}^{-1}$
$a^0$	initial value of $a$ , $\text{m}^{-1}$
$c_i$	concentration of species $i$ , $\text{mol}/\text{m}^3$
$c_{\text{init}}$	initial concentration of electrolyte, $\text{mol}/\text{m}^3$
$c_{i,\text{ref}}$	reference concentration of species $i$ , $\text{mol}/\text{m}^3$
$C_{ii}$	diagonal element of approximate Hessian
$D$	diffusion coefficient of the binary electrolyte, $\text{m}^2/\text{s}$
$E$	cell voltage, V
$F$	Faraday's constant, 96487 C/mol of electrons
$i_k$	current density due to electrochemical reaction $k$ , $\text{A}/\text{m}^2$
$i_{ok,\text{ref}}$	exchange current density of electrochemical reaction $k$ at $c_{\text{ref}}$ , $\text{A}/\text{m}^2$
$j$	current transferred between phases, $\text{A}/\text{m}^3$
$n$	number of data points
$n_k$	number of electrons transferred in the electrochemical reaction $k$
$m$	number of parameters
$P_i$	parameter $i$
$q_{ik}$	cathodic reaction order of species $i$ in reaction $k$
$R$	universal gas law constant, 8.314 J/mol-K
$s_E$	estimate of the variance of the residual error
$s_{P_i}$	estimate of the variance in the estimate of $P_i$
$S_l$	thickness of region $l$ , m
$SC_i$	sensitivity coefficient for parameter $i$
$SSR$	sum of squares of the residual error
$T$	cell temperature, K
$t_j$	time $j$ , sec
$\Delta t_{\text{max}}$	maximum time step, sec
$t_i^\square$	transference number of species $i$
$U_{k,\text{ref}}$	open circuit potential of reaction $k$ based on the reference concentrations, V

## Greek

$\alpha_{ak}$	anodic transfer coefficient for reaction $k$
$\alpha_{ck}$	cathodic transfer coefficient for reaction $k$
$\epsilon$	porosity of porous material
$\epsilon^0$	initial porosity of the porous electrode
$\eta_k$	overpotential for reaction $k$ at electrode surface ( $V - \Phi_o - U_{k,\text{ref}}$ ), V
$\xi$	morphology parameter
$\Phi$	solution potential, V
$\Phi_o$	solution potential at electrode surface, V

## REFERENCES

1. D. H. Johnson, A. D. Ayers, R. L. Zupancic, V. S. Alberto, and J. C. Bailey, *J. Power Sources*, **12**, 61 (1984).
2. S. Surampudi, G. Halpert, and I. Stein, "Safety Considerations of Lithium-Thionyl Chloride Cells," JPL publication 86-15 (June 1986).
3. T. I. Evans, T. V. Nguyen, and R. E. White, submitted for publication in the *J. Electrochem. Soc.*
4. K. A. Klinedinst and M. J. Domeniconi, *J. Electrochem. Soc.*, **127**, 539 (1980).
5. J. R. Driscoll, G. L. Holleck, and D. E. Toland, Proceedings of the 27<sup>th</sup> Power Sources Symposium, **28**, (1976).
6. H. Gu, T. V. Nguyen, and R. E. White, "A Mathematical Model for the Lead-Acid Cell: Discharge, Rest, and Charge," in press.
7. R. E. White, S. E. Lorimer, and R. Darby, *J. Electrochem. Soc.*, **130**, 1123 (1983).
8. J. S. Dunning, Ph.D. Dissertation, University of California, Los Angeles, CA (1971).
9. J. S. Dunning, D. N. Bennion, and J. Newman, *J. Electrochem. Soc.*, **120**, 906 (1973).
10. J. S. Newman, "Electrochemical Systems," Prentice Hall, Inc., Englewood Cliffs, NJ (1973).
11. P. E. Gill, W. Murray, and M. H. Wright, "Practical Optimization," Academic Press, New York, NY (1981).
12. T. V. Nguyen, Ph.D. Dissertation, Texas A&M University, College Station, TX (1988).
13. IMSL User's Manual, Edition 9.2, International Mathematical and Statistical Libraries, Inc. (1984).
14. B. Ostle and R. W. Mensing, "Statistics in Research," The Iowa State University Press, Ames, Iowa (1975).
15. T. I. Evans, Ph.D. Dissertation, Texas A&M University, College Station, TX (1988).
16. J. J. Auborn, K. W. French, S. I. Lieberman, V. K. Shah, and A. Heller, *J. Electrochem. Soc.*, **120**, 1613 (1973).
17. W. K. Behl, J. A. Christopoulos, M. Ramirez, and S. Gilman, *J. Electrochem. Soc.*, **120**, 1619 (1973).
18. K. M. Abraham, L. Pitts, and W. P. Kilroy, *J. Electrochem. Soc.*, **132**, 2301 (1985).
19. A. N. Dey, *J. Electrochem. Soc.*, **126**, 2052 (1979).
20. K. A. Klinedinst, *J. Electrochem. Soc.*, **132**, 2044 (1985).
21. A. N. Dey, *Electrochimica Acta.*, **21**, 377 (1976).

Table I. Model inputs used to simulate a 1 mA/cm<sup>2</sup> discharge of an experimental test cell (4).

Numerical parameters:		
Total number of node points	=	21
Maximum time step ( $\Delta t_{max}$ )	=	2000 seconds
Physical properties and initial conditions:		
Cell temperature ( $T$ )	=	25°C
Initial electrolyte concentration ( $c_{init}$ )	=	1.8 M
Reference electrolyte concentration ( $c_{ref}$ )	=	1.8 M
Transference number ( $t_+^{\#}$ )	=	0.9
All other values as in Tables I and II of ref. 3.		
Cell dimensions:		
Thickness of cathode ( $S_{pe}$ )	=	0.05 cm
Initial porosity of cathode ( $\epsilon^o$ )	=	0.845
Thickness of separator ( $S_s$ )	=	0.0127 cm
Porosity of separator ( $\epsilon_s$ )	=	0.7
Thickness of reservoir ( $S_r$ )	=	0 cm
Thickness of film ( $S_f$ )	=	0 cm
Lithium oxidation electro-kinetic parameters:		
$i_{o,1,ref}$	=	0.002 mA/cm <sup>2</sup>
$\alpha_{a,1}$	=	0.5
$\alpha_{c,1}$ ( = 1 - $\alpha_{a,1}$ )	=	0.5
$q_{+,1}$	=	1.0
SOCl <sub>2</sub> reduction electro-kinetic parameters:		
$a^o i_{o,4,ref}$	=	0.005 mA/cm <sup>3</sup>
$\alpha_{c,4}$	=	1.0
$\alpha_{a,4}$ ( = 2 - $\alpha_{c,4}$ )	=	1.0
$\xi$	=	0.05
$q_{+,4}$	=	1.0
$q_{o,4}$	=	0.5

Table II. Estimated values of the  $\text{SOCl}_2$  reduction electro-kinetic parameters using high rate ( $31 \text{ mA/cm}^2$ ) simulated data with added noise.

Actual Values*: $a^o i_{o,4,ref} = 0.0441 \text{ A/cm}^3$ $\alpha_{c,4} = 0.6846$ $\xi = 0.05$		
Z (mV)	Starting Values	Estimated Values (95% confidence, $\gamma = 0.05$ )
0.5	$\ln(a^o i_{o,4,ref}) = -5.423$ $(a^o i_{o,4,ref} = 0.00441)$ $\alpha_{c,4} = 0.171$ $\xi = 0.01$	$-3.073 \pm .0609$ $\left( \begin{matrix} 0.0463 & +0.00291 \\ & -0.00274 \end{matrix} \right)$ $0.681 \pm 0.0361$ $0.0487 \pm 0.01356$

\* The lithium oxidation electro-kinetic parameters were held fixed here at the following values:

$$i_{o,1,ref} = 1.58 \times 10^{-3}$$

$$\alpha_{a,1} = 0.18$$

Table III. Condition numbers for the approximate Hessians of the least squares objective function for the 1 mA/cm<sup>2</sup> simulated discharge. Large condition numbers indicate parameter interaction.

Case	Approximate Hessian of	Condition Number
A	$\ln(a^o i_{o,4,ref})$ and $\alpha_{c,4}$	$5.62 \times 10^2$
B	$\ln(a^o i_{o,4,ref})$ , $\alpha_{c,4}$ , and $\xi$	$1.18 \times 10^5$
C	$\ln(a^o i_{o,4,ref})$ , $\alpha_{c,4}$ , $\xi$ , and $\alpha_{a,1}$	$1.14 \times 10^6$
D	$\ln(a^o i_{o,4,ref})$ , $\alpha_{c,4}$ , $\xi$ , $\alpha_{a,1}$ , and $\ln(i_{o,1,ref})$	$6.16 \times 10^7$
E	$\alpha_{a,1}$ and $\ln(i_{o,1,ref})$	$4.30 \times 10^1$
F	$\ln(a^o i_{o,4,ref})$ , $\alpha_{c,4}$ , $\alpha_{a,1}$ , and $\ln(i_{o,1,ref})$	$1.03 \times 10^6$
G	$\ln(a^o i_{o,4,ref})$ , $\alpha_{c,4}$ , $\xi$ , $\alpha_{a,1}$ , $\ln(i_{o,1,ref})$ , $q_{+,1}$ , $q_{+,4}$ , and $q_{o,4}$	$2.45 \times 10^{12}$

Table IV. Estimated values of the lithium oxidation electro-kinetic parameters using simulated 1 mA/cm<sup>2</sup> data with added noise.

Actual Values: $i_{o,1,ref} = 0.002 \text{ A/cm}^2$ (Case E) $\alpha_{a,1} = 0.5$		
$Z \text{ (mV)}$	Starting Values	Estimated Values (95% confidence, $\gamma = 0.05$ )
0.5	$\ln(i_{o,1,ref}) = -8.517$	$-6.223 \pm .062$
	$(i_{o,1,ref} = 2.0 \times 10^{-4})$	$\begin{pmatrix} 0.00198 & +1.27 \times 10^{-4} \\ & -1.19 \times 10^{-4} \end{pmatrix}$
	$\alpha_{a,1} = 0.15$	$0.508 \pm 0.072$
1.0	$\ln(i_{o,1,ref}) = -8.517$	$-6.144 \pm 0.105$
	$(i_{o,1,ref} = 2.0 \times 10^{-4})$	$\begin{pmatrix} 0.002145 & +2.375 \times 10^{-4} \\ & -2.139 \times 10^{-4} \end{pmatrix}$
	$\alpha_{a,1} = 0.15$	$0.432 \pm 0.126$
1.0	$\ln(i_{o,1,ref}) = -10.82$	$-6.144 \pm 0.100$
	$(i_{o,1,ref} = 2.0 \times 10^{-5})$	$\begin{pmatrix} 0.002146 & +2.256 \times 10^{-4} \\ & -2.042 \times 10^{-4} \end{pmatrix}$
	$\alpha_{a,1} = 0.85$	$0.432 \pm 0.118$
2.0	$\ln(i_{o,1,ref}) = -8.517$	$-6.263 \pm 0.211$
	$(i_{o,1,ref} = 2.0 \times 10^{-4})$	$\begin{pmatrix} 0.001906 & +4.476 \times 10^{-4} \\ & -3.625 \times 10^{-4} \end{pmatrix}$
	$\alpha_{a,1} = 0.15$	$0.5337 \pm 0.248$

Table V. Estimated values of the exchange current density and transfer coefficient of the  $\text{SOCl}_2$  reduction reaction using simulated  $1 \text{ mA/cm}^2$  data with added noise.

Actual Values: $a^o i_{o,4,ref} = 0.005 \text{ A/cm}^2$ (Case A) $\alpha_{c,4} = 1.0$		
$Z \text{ (mV)}$	Starting Values	Estimated Values (95% confidence, $\gamma = 0.05$ )
0.5	$\ln(a^o i_{o,4,ref}) = -2.996$	$-5.293 \pm 0.0732$
	$(a^o i_{o,4,ref} = 0.05)$	$\begin{pmatrix} 0.00503 & +3.82 \times 10^{-4} \\ & -3.55 \times 10^{-4} \end{pmatrix}$
	$\alpha_{c,4} = 0.25$	$0.9981 \pm 0.0212$
0.5	$\ln(a^o i_{o,4,ref}) = -9.903$	$-5.293 \pm 0.0732$
	$(a^o i_{o,4,ref} = 5.0 \times 10^{-5})$	$\begin{pmatrix} 0.00503 & +3.82 \times 10^{-4} \\ & -3.55 \times 10^{-4} \end{pmatrix}$
	$\alpha_{c,4} = 1.75$	$0.9981 \pm 0.0212$
1.0	$\ln(a^o i_{o,4,ref}) = -0.6931$	$-5.239 \pm 0.123$
	$(a^o i_{o,4,ref} = 0.5)$	$\begin{pmatrix} 0.0053 & +6.948 \times 10^{-4} \\ & -6.144 \times 10^{-4} \end{pmatrix}$
	$\alpha_{c,4} = 0.25$	$0.9842 \pm 0.0357$
2.0	$\ln(a^o i_{o,4,ref}) = -9.903$	$-5.212 \pm 0.234$
	$(a^o i_{o,4,ref} = 5.0 \times 10^{-5})$	$\begin{pmatrix} 0.00545 & +0.00144 \\ & -0.00114 \end{pmatrix}$
	$\alpha_{c,4} = 1.75$	$0.9727 \pm 0.0677$

Table VI. Estimated values of the  $\text{SOCl}_2$  reduction electro-kinetic parameters using simulated  $1 \text{ mA/cm}^2$  data with added noise.

Actual Values: $a^o i_{o,4,ref} = 0.005 \text{ A/cm}^3$ (Case B) $\alpha_{c,4} = 1.0$ $\xi = 0.05$		
Z (mV)	Starting Values	Estimated Values (95% confidence, $\gamma = 0.05$ )
0.5	$\ln(a^o i_{o,4,ref}) = -7.601$	$-5.289 \pm .129$
	$(a^o i_{o,4,ref} = 5.0 \times 10^{-4})$	$\begin{pmatrix} 0.00505 & +6.95 \times 10^{-4} \\ & -6.11 \times 10^{-4} \end{pmatrix}$
	$\alpha_{c,4} = 0.25$	$1.001 \pm 0.075$
	$\xi = 0.01$	$0.0494 \pm 0.0184$
1.0	$\ln(a^o i_{o,4,ref}) = -9.903$	$-5.257 \pm .189$
	$(a^o i_{o,4,ref} = 5.0 \times 10^{-5})$	$\begin{pmatrix} 0.00521 & +1.085 \times 10^{-3} \\ & -8.98 \times 10^{-4} \end{pmatrix}$
	$\alpha_{c,4} = 1.75$	$0.9707 \pm 0.1238$
	$\xi = 0.01$	$0.0535 \pm 0.0313$

Table VII. Estimated values of all five electro-kinetic parameters describing the Li/SOCl<sub>2</sub> cell using simulated 1 mA/cm<sup>2</sup> data with added noise.

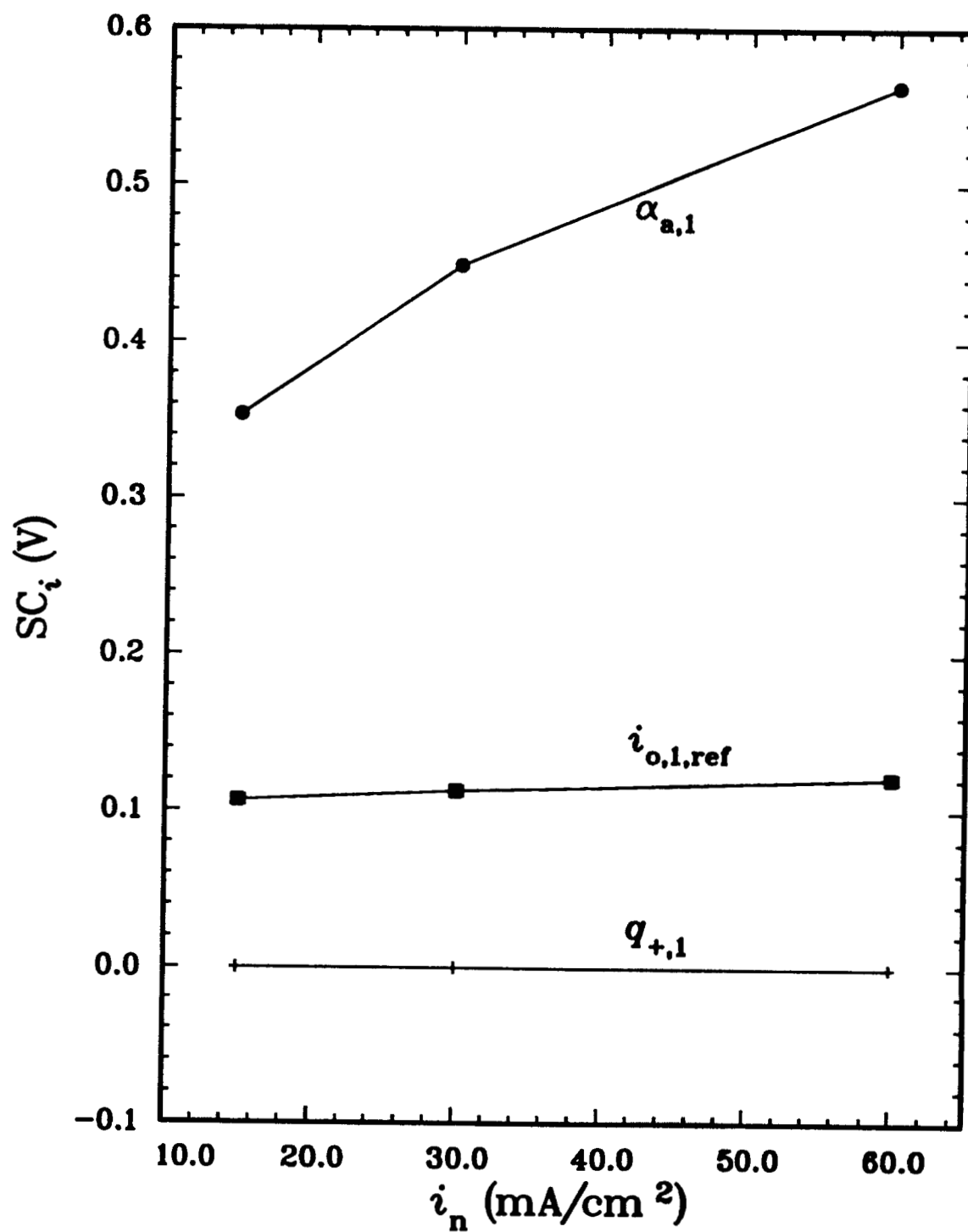
Actual Values: $a^o i_{o,4,ref} = 0.005 \text{ A/cm}^3$ (Case D)		
$\alpha_{c,4} = 1.0$		
$\xi = 0.05$		
$i_{o,1,ref} = 0.002 \text{ A/cm}^2$		
$\alpha_{a,1} = 0.5$		
Z (mV)	Starting Values	Estimated Values (95% confidence, $\gamma = 0.05$ )
0.0	$\ln(a^o i_{o,4,ref}) = -7.601$	-5.298
	$(a^o i_{o,4,ref} = 5.0 \times 10^{-4})$	$(5.0 \times 10^{-4})$
	$\alpha_{c,4} = 0.5$	1.00
	$\xi = 0.025$	0.05
	$\ln(i_{o,1,ref}) = -8.517$	-6.215
	$(i_{o,1,ref} = 2.0 \times 10^{-4})$	$(2.0 \times 10^{-4})$
	$\alpha_{a,1} = 0.25$	0.5
	SSR = $1.0 \times 10^{-18}$	
0.5	$\ln(a^o i_{o,4,ref}) = -7.601$	$-5.031 \pm 2.078$
	$(a^o i_{o,4,ref} = 5.0 \times 10^{-4})$	$\begin{pmatrix} 0.00653 & +0.0457 \\ & -0.00571 \end{pmatrix}$
	$\alpha_{c,4} = 0.5$	$1.00 \pm 0.253$
	$\xi = 0.025$	$0.0656 \pm 0.0678$
	$\ln(i_{o,1,ref}) = -8.517$	$-6.523 \pm 1.292$
	$(i_{o,1,ref} = 2.0 \times 10^{-4})$	$\begin{pmatrix} 0.00147 & +0.00388 \\ & -0.00107 \end{pmatrix}$
	$\alpha_{a,1} = 0.25$	$0.374 \pm 1.80$
	SSR = $1.067 \times 10^{-5}$	

Table VIII. Estimated values of the  $\text{SOCl}_2$  reduction electro-kinetic parameters of the  $\text{Li}/\text{SOCl}_2$  cell using available experimental data at  $31 \text{ mA}/\text{cm}^2$ .

SSR	Starting Values	Estimated Values (95% confidence, $\gamma = 0.05$ )
Run # 1 (Case B)		
$0.95 \times 10^{-4}$	$\ln(a^o i_{o,4,ref}) = -3.0$	$-1.51 \pm 5.78$
	$(a^o i_{o,4,ref} = 0.05)$	$\begin{pmatrix} 0.221 & +71.3 \\ & -0.22 \end{pmatrix}$
	$\alpha_{c,4} = 0.5$	$0.657 \pm 0.134$
	$\xi = 0.05$	$0.0112 \pm 0.0724$
Run # 2 (Case B)		
$0.96 \times 10^{-4}$	$\ln(a^o i_{o,4,ref}) = -7.601$	$-2.3 \pm 1.95$
	$(a^o i_{o,4,ref} = 5.0 \times 10^{-4})$	$\begin{pmatrix} 0.100 & +0.604 \\ & -0.086 \end{pmatrix}$
	$\alpha_{c,4} = 1.5$	$0.64 \pm 0.139$
	$\xi = 0.1$	$0.028 \pm 0.0736$
Run # 3 (Case E)		
$0.95 \times 10^{-4}$	$\ln(a^o i_{o,4,ref}) = -3.0$	$-2.00 \pm 0.655$
	$(a^o i_{o,4,ref} = 0.05)$	$\begin{pmatrix} 0.135 & +0.125 \\ & -0.065 \end{pmatrix}$
	$\alpha_{c,4} = 0.5$	$0.646 \pm 0.094$

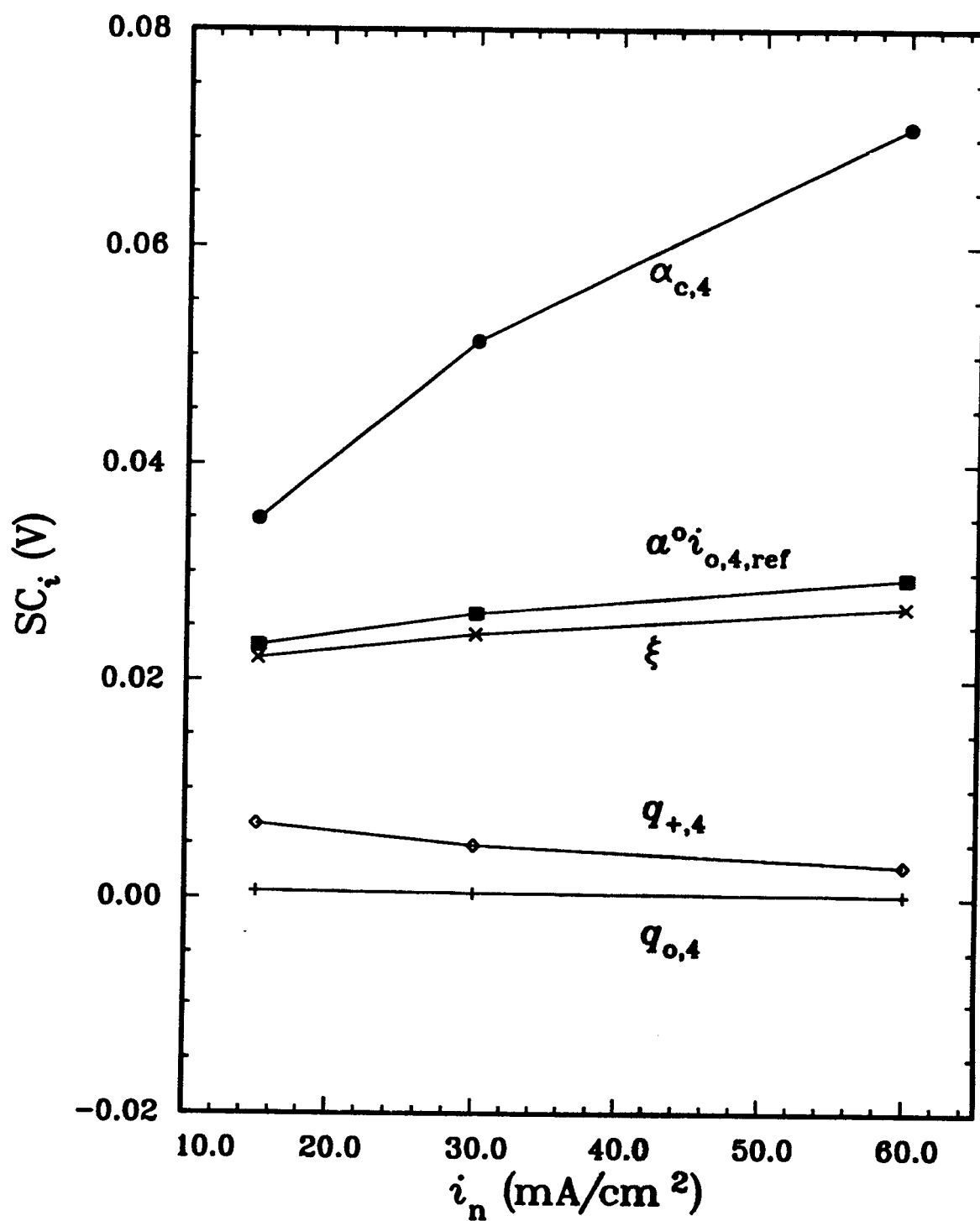
## LIST OF FIGURE CAPTIONS

- Fig. 1 Sensitivity of the predicted cell voltage to changes in the electro-kinetic parameters characterizing the lithium oxidation, reaction [1].
- Fig. 2 Sensitivity of the predicted cell voltage to changes in the electro-kinetic parameters characterizing the  $\text{SOCl}_2$  reduction, reaction [4].
- Fig. 3 Sensitivity of the predicted cell voltage to changes in the transport parameters characterizing migration ( $t_+^\oplus$ ) and diffusion ( $\beta_6$ ) of the electrolyte.
- Fig. 4 Time-dependent sensitivity coefficients for a  $31 \text{ mA/cm}^2$  simulated discharge evaluated at the exact values of the electro-kinetic parameters. Parallel lines indicate parameter interaction.
- Fig. 5 Time-dependent sensitivity coefficients for a  $1 \text{ mA/cm}^2$  simulated discharge evaluated at the exact values of the electro-kinetic parameters.
- Fig. 6 A simulated  $1 \text{ mA/cm}^2$  discharge of a  $\text{Li/SOCl}_2$  cell with three levels of added random noise.
- Fig. 7 A comparison of model predictions to experimental data at  $31 \text{ mA/cm}^2$ . Electro-kinetic parameters are as shown in Table VIII, Run # 1.



Evers and White

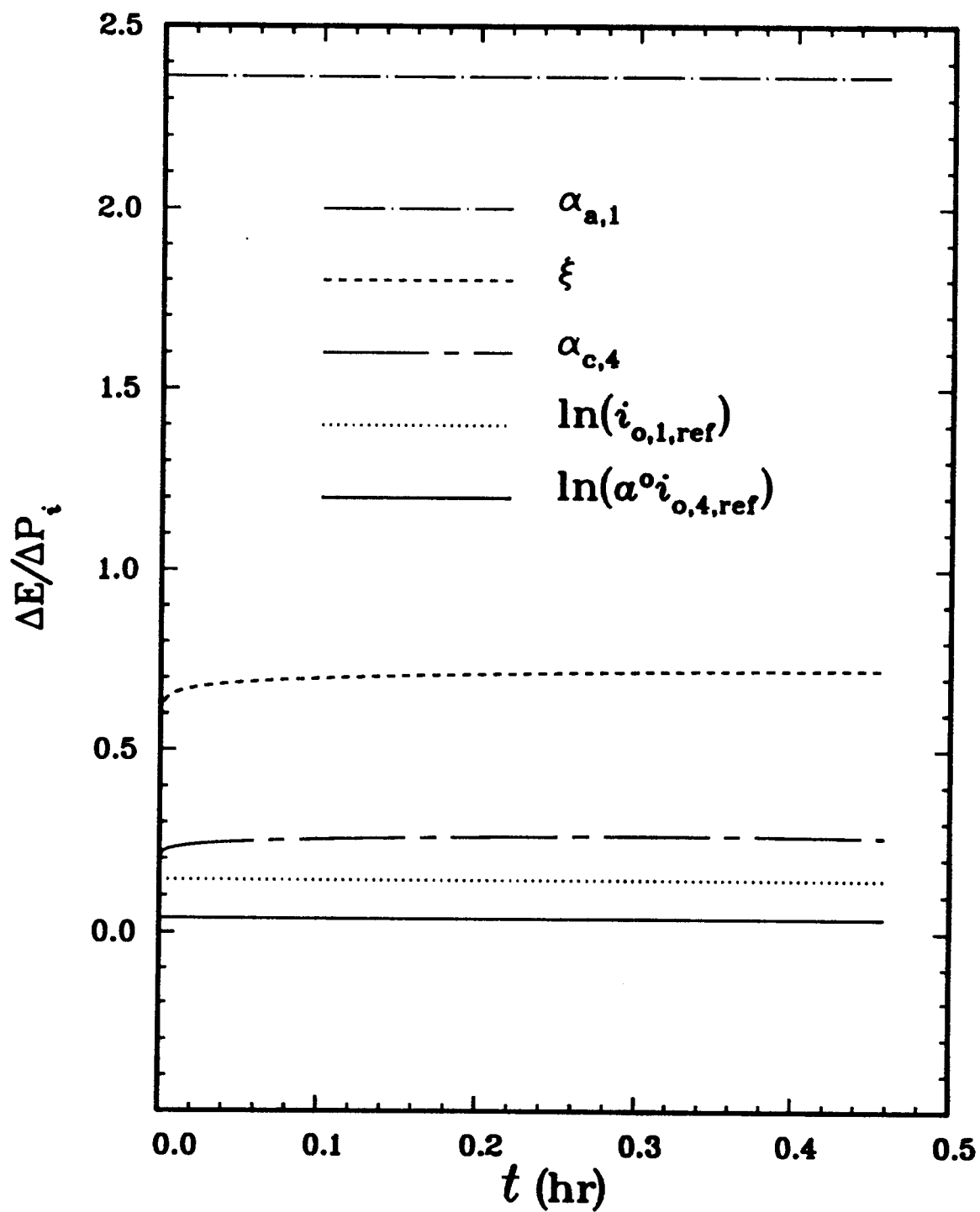
Fig. 1



Ercevic and White

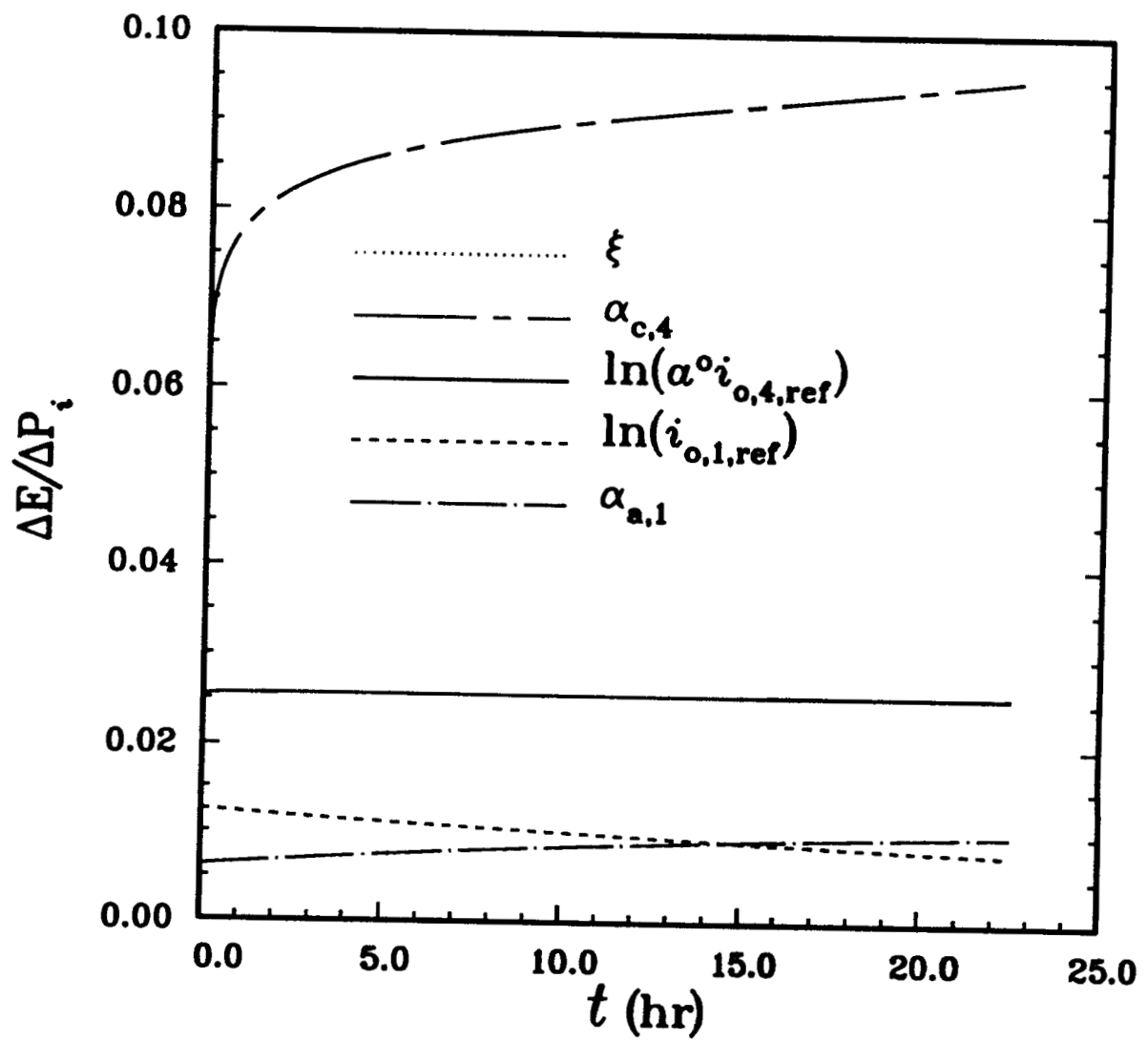
Fig. 2





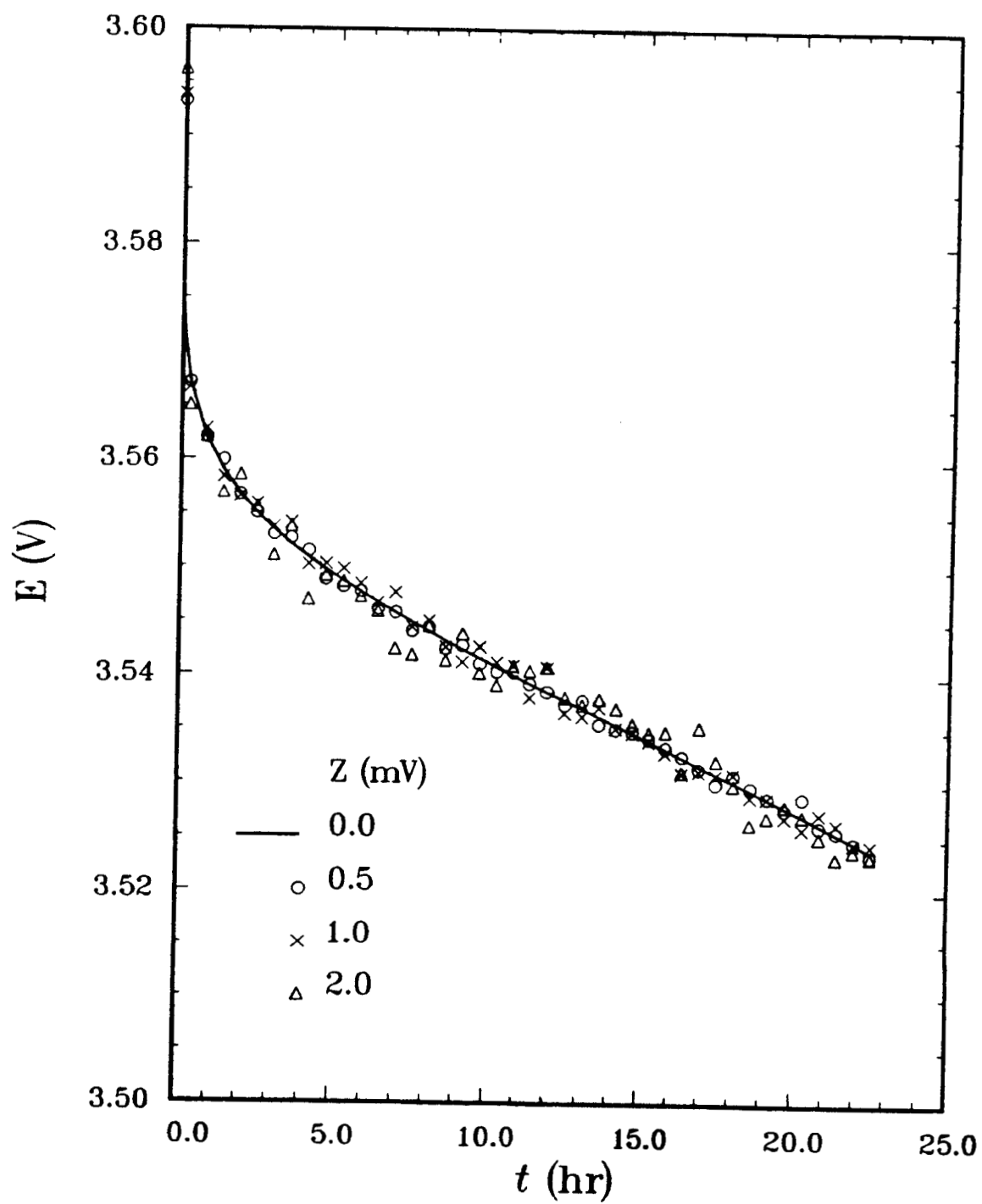
Evans and White

Fig. 4



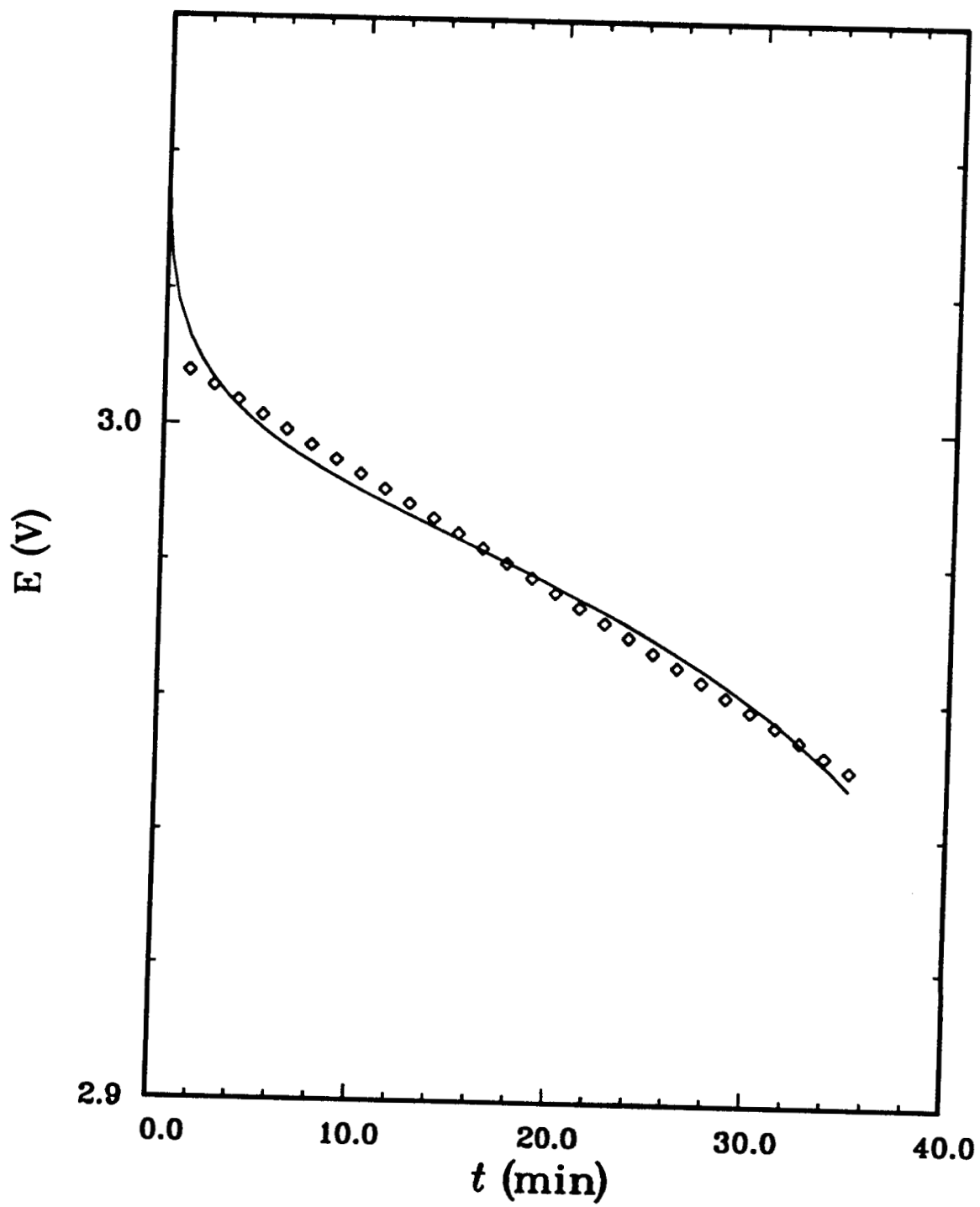
Evans and White

Fig. 5



*Exponential decay*

Fig. 6



*Exponential fit to*

*Fig 5*



## APPENDIX B

**A Thermal Analysis of a Spirally Wound Battery Using a  
Simple Mathematical Model**

by

T. I. Evans\* and R. E. White\*\*

Department of Chemical Engineering

Texas A&M University

College Station, Texas 77843

submitted as a technical paper

to the

Editor

Journal of the Electrochemical Society

10 South Main Street

Pennington, New Jersey 08534

April, 1988

**Key Words:** discharge, energy balance, lithium/thionyl chloride, spiral, thermal runaway

---

\* Electrochemical Society Student Member

\*\*Electrochemical Society Active Member

ABSTRACT

A two-dimensional thermal model for spirally wound batteries has been developed. The governing equation of the model is the energy balance. Convective and insulated boundary conditions are used and the equations are solved using a finite element code called TOPAZ2D. The finite element mesh is generated using a preprocessor to TOPAZ2D called MAZE. The model is used to estimate temperature profiles within a spirally wound D-size cell. The model is applied to the lithium/thionyl chloride cell because of the thermal management problems that this cell exhibits. Simplified one-dimensional models are presented which can be used to predict best and worst temperature profiles. The two-dimensional model is used to predict the regions of maximum temperature within the spirally wound cell. Normal discharge as well as thermal runaway conditions are investigated.

## INTRODUCTION

Many battery systems produce heat as they are discharged due to the exothermic nature of the electrochemical reactions occurring. This build up of heat can result in dangerous conditions depending upon the cell design and physical system. Often, thermal modeling of these battery systems is accomplished by assuming that the different components of the battery interior can be represented by a homogeneous region (i.e. core region) having average properties. This approach is useful because it greatly simplifies the analysis, however, it may not provide adequate results when the different components of the battery have vastly different thermal properties. Often, the material used for separating the anode from the cathode has a much lower thermal conductivity than the electrodes themselves. This condition may lead to heat management problems in spirally wound designs when the heat flow is primarily in the radial direction. Heat management could be improved in the spiral design if heat flow can proceed out the spiral along the more conductive materials; however, the spiral path offers a much greater distance to traverse as opposed to the more direct radial path. This work shows that conduction of heat out the spiral, during normal operation, reduces cell temperatures but does not substantially reduce the temperature drop in the cell. However, when hot spots are present in the cell conduction out the spiral is substantial and the temperature drop in the cell is reduced significantly.

The  $\text{Li/SOCl}_2$  cell is an example of a spirally wound D-size cell that has a thermal management problem. It is an attractive primary energy source because of its high energy density (1, 2). However, researchers have observed that high discharge rates and high temperatures promote thermal runaway in these cells (1-5). Venting of toxic gases and explosions, due to the rapid pressure build up at higher temperatures, have been reported (1-5).

The purpose of this paper is to present a model that can be used to predict temperature profiles, in time and two spatial dimensions, within a spirally wound D-size Li/SOCl<sub>2</sub> cell and to estimate the ability of this design to conduct heat out of the cell. One-dimensional approximations to the two-dimensional analysis will be investigated for comparison purposes. Predictions from a one-dimensional model for a C-size cell are compared with experimental data (6) to learn more about the thermal behavior of Li/SOCl<sub>2</sub> cells. Finally, hypothetical thermal runaway situations are simulated using the two-dimensional model and a one-dimensional approximation in order to determine if the spiral design offers any thermal advantage under such conditions.

#### *Description of a spirally wound electrochemical cell*

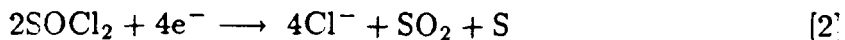
Figures 1 and 2 show two different views of a spirally wound electrochemical cell. The cell is constructed by inserting the cell roll into a cylindrical can as shown in Fig. 1. Electrolyte is poured into the can and fills the porous regions of the roll so that a reservoir of electrolyte remains at the top of the roll. Electrodes are constructed by impregnating the electrode materials on the both sides of the current collector mesh (usually a nickel mesh in the Li/SOCl<sub>2</sub> cell). The anode current collector is usually spot welded to the side of the can and tabs connected to the cathode current collector are welded to the center post protruding through the can lid. The cell roll is constructed by stacking the anode, separator, and cathode on top of each other and then rolling up the stack. A top view of the roll is shown in Fig. 2 - which is the two-dimensional plane of interest. The current collectors, embedded in the middle of each electrode, are not shown in Fig. 1 or 2.

#### *Description of a Li/SOCl<sub>2</sub> cell*

In a typical Li/SOCl<sub>2</sub> cell, the anode is Lithium, the cathode is a porous carbon structure, and the separator is a glass matting material. The electrolyte consists of lithium tetrachloroaluminate (LiAlCl<sub>4</sub>) in thionyl chloride (SOCl<sub>2</sub>). During discharge, Li is oxidized



and SOCl<sub>2</sub> is reduced



The SOCl<sub>2</sub> is the active material at the cathode; the porous carbon structure provides the sites upon which the SOCl<sub>2</sub> is reduced. This redox couple generates heat as the cell is discharged and this heat must be conducted away at a fast enough rate so that unsafe conditions will not develop.

This brief description is a simple analysis of the actual physical system. It has been observed that the Li/SOCl<sub>2</sub> cell is a complex chemical and electrochemical system involving an unknown number of reactions (2). Szpak and Venkatsetty (7) state that modeling the Li/SOCl<sub>2</sub> cell is difficult due to the complexity of this physical system. They observe that as the cell discharges, the temperature and pressure of the cell change, the volume of electrolyte decreases, the electrolyte composition varies, and new phases appear. However, much can be learned by modeling a simplified picture of the actual system.

### *Previous models*

Previous workers (8, 9) have presented thermal models for battery systems. Bernardi *et al.* (8) give an excellent development of a general energy balance for electrochemical systems. They present a complete energy balance which requires the knowledge of concentration profiles and current fractions within the cell. However, the energy balance is formulated by assuming that the temperature of the battery is

uniform and changes only with time. That is, flat temperature profiles are assumed *a priori*. Lee *et al.* (9) present a three-dimensional model for battery systems involving a number of batteries in one unit. However, they treat the interior region of each battery as a homogeneous phase having effective average properties. Therefore the model cannot be used to predict the effects of the arrangement of the cell components on the temperature distribution.

Several models (10-19) have been presented which specifically address the thermal behavior of Li/SOCl<sub>2</sub> cells. Parnell and Szpak (10) present a thermal model for thin, disc-shaped Li/SOCl<sub>2</sub> cells in one dimension. They consider heat generation due to the polarization of the electrodes and internal cell resistance. A differential energy balance, which includes various terms representing different contributions to the heat generation, is solved numerically to obtain temperature profiles within the cell. Their model is used to show that as the rate of discharge is increased, the temperature increase is proportional to the increase in cell current. Szpak *et al.* (11) present a one-dimensional thermal model for disc-shaped Li/SOCl<sub>2</sub> cells, similar to the model by Parnell and Szpak (10), which accounts for catastrophic thermal runaway. This model is formulated by associating thermal runaway with ignition and burning, via one or more cell defects, rather than explosion. A differential energy balance and a differential material balance, which includes diffusion of species only, are solved simultaneously using a numerical method. The model is used to predict the time and position dependent temperature and concentration profiles. The model predictions compare favorably to what is physically observed which may indicate that the reactions causing thermal runaway are initiated by localized heat sources developed from defective cells or cell components. Cho and Halpert (12) have presented a simple thermal model for spirally wound Li/SOCl<sub>2</sub> primary cells. In this work, an energy balance which requires an experimentally determined term for the heat generation rate is solved

analytically to obtain the temperature of the cell as a function of time. They assume a uniform cell temperature which changes with time as has been done by a number of workers (8, 13-16). Cho and Halpert (18) and Cho (19) have taken the modeling one step further by developing a means to calculate the heat generation rate term in their model (12) using experimentally determined resistances. An electrical circuit analogue is used which consists of the thermal resistances of the various cell components. None of these models can be used here because each model treats the cell interior as one, pseudohomogenous material.

Other Li/SOCl<sub>2</sub> cell models have been developed (13-17). Evans *et al.* (13) and Tsaur and Pollard (14-17) use conservation of mass and charge to determine the concentration and reaction rate profiles in the cell. Both use porous electrode theory (20, 21) and concentrated solution theory (22-24) to develop the governing equations in one dimension. Evans *et al.* (13) include four cell regions in their model whereas Tsaur and Pollard (14) essentially treat two cell regions. The boundary conditions used in each model are different and are based on different simplifying assumptions. It is assumed in each model that the cell temperature is uniform at any given moment in time. The cell temperature change with time is predicted using an overall energy balance. Tsaur and Pollard (15, 16) extend their model to include the additional species present when an acid electrolyte is utilized, such as in reserve cells (25). However, these previous models cannot be used to investigate the two-dimensional temperature profiles in spirally wound Li/SOCl<sub>2</sub> cells.

## MODEL FORMULATION

The differential energy balance for region  $k$  of a battery can be written as

$$\rho_k c_{p,k} \frac{\partial T}{\partial t} = \nabla \cdot (\lambda_k \nabla T) + \sum_j \dot{q}_j''' \quad (j = 1, 2, \dots) \quad [3]$$

where  $c_{p,k}$  and  $\lambda_k$  are the heat capacity and thermal conductivity of region  $k$ , respectively. In some instances, the steady state temperature profiles are of interest in which case the term  $\partial T / \partial t$  in Eq. [3] is set to zero. The  $\dot{q}_j'''$  terms in Eq. [3] represent various heat sources and sinks. Heat generated by polarization ( $\dot{q}_p'''$ ) and heat generated due to the entropy change of the current producing reactions ( $\dot{q}_s'''$ ), reactions 1 and 2, will be included in Eq. [3] for normal discharge conditions. The heat generation terms  $\dot{q}_p'''$  and  $\dot{q}_s'''$  are calculated as follows (26, 27)

$$\dot{q}_p''' + \dot{q}_s''' = \frac{\dot{q}_p + \dot{q}_s}{V_{cell}} \quad [4]$$

where

$$\dot{q}_p + \dot{q}_s = I \left( E_{oc} - E - T \frac{dE_{oc}}{dT} \right) = I(E_{tn} - E) \quad [5]$$

$E_{tn}$  in Eq. [5], termed the thermoneutral potential, is the theoretical open circuit potential of the cell at absolute zero. The cell voltage,  $E$  in Eq. [5], must be specified and can be obtained from experiment or predicted using an earlier model (13). Other sources/sinks of heat would include exothermic or endothermic chemical reactions occurring in the cell which do not produce current (27). These sources are assumed to be negligible in this paper as is usually done for normal operation. To simulate thermal runaway, an additional  $\dot{q}_d'''$  term is included in Eq. [3],  $\dot{q}_d'''$ , representing additional heating caused by, perhaps, a cell defect and/or exothermic chemical reactions. This heat source is assumed to be localized causing a hot spot in the cell. This approach to simulating thermal runaway was used by Szpak *et al.* (11).

To complete the mathematical description of the cell, the boundary conditions must be specified. For the cases investigated here, either a zero flux (insulated) boundary condition

$$\lambda_{k,x} \frac{\partial T}{\partial x} \mathbf{n}_x + \lambda_{k,y} \frac{\partial T}{\partial y} \mathbf{n}_y = 0 \quad [6]$$

or a convection boundary condition

$$-\lambda_{k,x} \frac{\partial T}{\partial x} \mathbf{n}_x - \lambda_{k,y} \frac{\partial T}{\partial y} \mathbf{n}_y = h(T_w - T_A) \quad [7]$$

is used. In Eq. [7],  $T_w$  is the temperature of the cell at its outer wall and is a function of  $x$ ,  $y$ , and  $t$ ,  $T_A$  is the surrounding temperature and is a fixed value, and  $h$  is a heat transfer coefficient. It is assumed here, for simplicity, that  $h$  is a constant and adequately characterizes the heat transfer through the cell casing and from the case wall to the surroundings via convection.

## SOLUTION PROCEDURE

The finite element method (28, 29) is used to solve numerically Eq. [3], with Eq. [6] and [7], for the model region shown in Fig. 3. The computer package called TPAZ2D (29) is used. Input files to TOPAZ2D, containing the coordinates of the finite element mesh, are created using another computer program called MAZE (30).

In order to obtain reliable, consistent results using the finite element method, a smooth mesh must be constructed and nodal points at region interfaces must match up. To achieve this, the two-dimensional spiral mesh is developed by constructing two semicircular meshes, offsetting one semicircular mesh, and then joining the two meshes together. A schematic of a model region constructed in this way is shown in Fig. 3 where  $x$  and  $y$  are the orthogonal vectors defining the two-dimensional plane and which intersect at the origin. The vector  $x_1$  is shown in Fig. 3 because a temperature profile along this vector is shown later in this paper. The left half consists of four concentric semicircular cells and the right half consists of three concentric semicircular cells. Comparison of Fig. 2 and Fig. 3 shows that this construction provides a reasonable representation of the spiral design. For normal discharge conditions, meshes were refined until three digit accuracy was obtained.

Table I lists the cell specifications for the spirally wound design investigated here. A similar cell is currently being developed by Wilson-Greatbatch (31) and may be used for applications in space (32). The thermophysical properties of each cell region and other model inputs are listed in Table II. Note that the properties for the cathode region and separator region are average properties calculated by assuming that all voids are filled with electrolyte. Here, the porous cathode was assumed to be 85 % porous and the separator 70 % porous.

## RESULTS AND DISCUSSION

Two simplified cases of the spiral design were investigated. The spiral was approximated using concentric circular regions, the top schematic in Fig. 4. and a core region, the bottom schematic in Fig. 4. The core region approach is based on the assumption that the cell interior can be represented by one homogeneous region. This core region possesses thermophysical properties which are the average of the properties of all the cell components. The core region properties were calculated as follows

$$\bar{p} = \frac{\sum_i \delta_i p_i}{\sum_i \delta_i} \quad [8]$$

where  $\delta_i$  is the thickness of region  $i$  and  $p_i$  is the value of a thermophysical property of region  $i$  as listed in Table II. The core properties are listed in Table II. These two cases simplify the calculations because the governing equations need be solved in one dimension only. In fact, the steady state equation set for the core approach is easily solved analytically. Also, these two cases represent two different extremes. The circles case should yield a maximum temperature drop from the center of the cell to the cell exterior because all heat is forced to flow radially through all cell regions, including the separator region which offers the most resistance to heat flow. The core case should yield a minimum temperature drop from the center of the cell to the exterior because the thermophysical properties of the core region closely resemble those of the most conductive regions, as shown in Table II. The spiral case, as shown in Fig. 3, should yield temperature profiles somewhere between these two extremes. Heat flow in the radial direction is inhibited by the separator; however, heat can flow out the spiral along the more conductive materials. In the results which follow, the core approximation, the concentric circular regions approximation, and the spiral case are referred to as core, circles, and spiral, respectively.

### *Comparison of the core, circles, and spiral models:*

Figure 5 shows predicted time-temperature profiles for the core, circles, and spiral cases for a 4 A discharge. The heat generation rate program, shown in Fig. 6, was calculated using Eq. [5] and the voltage transient shown in Fig. 6. The voltage transient was approximated from experimental results reported in the literature (2, 6, 33). Voltage transients can also be predicted from earlier models (13, 14). It should be noted that there exists a wide range of data for the Li/SOCl<sub>2</sub> cell reported in the literature due to differences in the discharge rates, electrode materials, and cell designs investigated (2-6, 25, 33-36). Notice in Fig. 5 that the predicted maximum and minimum temperature dependence on time for the spiral case falls between those of the core and circles cases, as expected. Also note that the core case shows an essentially uniform cell temperature, whereas the circles and spiral cases show about a 2 K temperature drop from the cell interior ( $T_{\max}$ ) to the cell wall ( $T_{\min}$ ). The general shape of the curves are in qualitative agreement with experimental temperature-time curves (6), as shown in Fig. 9; an initial rise in temperature as the electrodes are first polarized, then a plateau is reached where heat generation is about equal to heat transfer away from the cell, then a sharp increase in cell temperature at the very end of the discharge. A comparison of model predictions presented here and experimental results (6) is made below.

The two-dimensional temperature profile for the spiral cell at approximately 1.5 hr of discharge (corresponding to the dot in Fig. 5) is shown in Fig. 7. The plotted points are the temperatures at each node point of the spiral mesh. The temperature is plotted over the two-dimensional plane defined by the orthogonal vectors  $x$  and  $y$  shown in Fig. 3. The maximum temperature is in the electrolyte region located near the center of the cell (see Fig. 3). As shown in Table II, the electrolyte possesses a low thermal conductivity and thus serves to retain heat relative to the other cell components. The temperature drops from this maximum

to the minimum temperature located at the outer corner of the spiral, point A in Fig. 3. The largest temperature drops are across the separator and appear as the void spaces between the various levels of the spiral.

Figure 8 compares spatial temperature profiles as predicted using the core, circles, and spiral methods. These profiles correspond to approximately 1.5 hr into the discharge, as shown by the box and dot in Fig. 5. Two profiles are shown for the spiral case, one along vector  $y$  and one along vector  $x_1$  corresponding to the vectors shown in Fig. 3. In order to better compare the profiles, the temperature difference  $T - T_{\min}$  is plotted on the ordinate. Figure 8 shows that the core approximation does not adequately predict the temperature drop in the spirally wound cell. In this case, the predicted temperature drop is about 2 K according to the spiral model whereas the core approximation yields only about a 0.2 K drop. Fig. 8 also shows that the profiles for the circles approximation and spiral case are in close proximity. The circles approximation is useful because it predicts maximum temperature profiles, as shown in Fig. 5 and 8, and is easily solved in one-dimension using TOPAZ2D.

Several items are noteworthy in the forgoing comparisons between the core, circles, and spiral cases. The spiral model region, shown in Fig. 3, has boundaries different from the core and circles model regions, shown in Fig. 4. The difference is the exposed end of the spiral cell between points A and B in Fig. 3. For the core and circles cases, Eq. [7] is used at the outer boundary. For the spiral, Eq. [7] is used for the outer boundary (clockwise from point A to point B in Fig. 3) and Eq. [6] is used for the end of the spiral cell (counterclockwise from point A to point B in Fig. 3). This use of insulated boundary conditions at the exposed end represents a worst case; in the actual cell, shown in Fig. 1, the lithium electrode is extended and the rest of the spiral end borders electrolyte. For comparison purposes, Eq. [7] was used for all boundaries of the spiral. The relative temperature drop from the cell interior to the exterior remained essentially the same, however, the absolute

temperature profile dropped about 1 K. What can be gleaned from this and the forgoing comparisons is that the spiral design aides in cooling down the cell, as opposed to the circles case, because heat can be conducted out the spiral path as well as out the radial direction. This increase reduces the cell temperatures but does not substantially reduce the temperature drop from the center of the cell to the cell wall.

Finally, the effect of different heat generation rate distributions on the temperature profiles was briefly investigated using the spiral model. Four cases were run: 90 % of the heat generation contained within the lithium anode and 10 % within the cathode, 10 % within the anode and 90 % within the cathode, 90 % within the separator and 10 % within the cathode, and 50 % within the anode and 50 % within the cathode. Each case yielded about a 2 K temperature drop.

*Comparison of circles model with experimental results:*

The one-dimensional circles model was used to simulate the temperature profiles for an experimental test case reported by Abraham *et al.* (6) for a C-size Li/SOCl<sub>2</sub> cell. The component dimensions, cell volume, and other test conditions given in their paper were used in the model; eight wraps were assumed. The heat generation rate program was calculated based on the voltage transients shown in Fig. 7 of their work. The value of the heat transfer coefficient was set to 15 W/m-K, instead of 10 W/m-K as in Table II, in order to match predictions to the experimental data as closely as possible.

The experimental temperature-time curves for the 4 A discharge of a catalyzed Li/SOCl<sub>2</sub> cell are shown in Fig. 9. The difference in cell temperature from the center of the cell to the can wall is shown to be as much as 13 K. Model predictions, not those shown in Fig. 9, show only about a 3 K to 4 K temperature drop. The model predictions given in Fig. 9 show about an 8 K temperature drop and

were obtained by making several changes to the model as described below. Several factors could account for the differences between the model predictions and the experimental measurements. First, this data is for a cell having porous cathodes containing 5 weight percent dibenzotetraazaannulene complex of cobalt (Co-TAA). These catalyzed cells exhibit discharge behavior different from uncatalyzed cells (6) and the heat generation rate, as predicted using Eq. [5] and the thermoneutral potential listed in Table II, used in the model may not be appropriate. Assuming that this difference has no effect on model predictions, several other factors may be considered. The heat generation within the cell may not be uniform; it is probable that heat generation is greatest near the center of the cell and diminishes in value when approaching the cell exterior. This can be explained by considering the current density; near the center of the spirally wound cell there exists less electrode area over which the radially flowing current is distributed than at radii further from the center of the cell. Thus the electrochemical reaction rate would be greatest at the center, evolving more heat at the center, and decrease from there to the cell exterior. Decreasing thermal conductivities could also explain these large temperature drops. As the cell is discharged, the  $\text{SOCl}_2$  electrolyte is reduced at the cathode and is sometimes depleted to the point where cell gases fill some of the voids previously occupied by electrolyte (32). To approximate these possibilities two changes were made to the model. The heat generation rate was set to a maximum value in the first concentric cell (relative value of 4) and was decreased linearly to a minimum value in the eighth concentric cell (relative value 1). The densities, heat capacities, and thermal conductivities of the regions containing electrolyte were changed by assuming that at the end of the discharge only  $\text{SO}_2$  remained in the void portions of these regions. These properties were changed linearly throughout the discharge from their starting values, reported in Table II, to their ending values, reported in Table III. The model predictions are superimposed on the experimental data

in Fig. 9. Agreement between predictions and experiment has been improved by these changes. Steeper heat generation rate profiles were tried, resulting in larger temperature drops, but the temperature-time relationships did not agree well with the experimental results in Fig. 9. It should be possible to improve the fit of the theoretical predictions to the experimental results by using a parameter estimation technique in conjunction with TOPAZ2D.

These differences between experiment and model indicate several possibilities. Perhaps a more detailed program for the heat generation rate is needed. Other chemical or electrochemical reactions could be occurring, especially at these high rates of discharge, which cause greater heat generation rates; these reactions could be localized. The thermal runaway simulations presented next were run with some of these thoughts in mind. More experimental data, including temperature measurements throughout the cell from center to wall, are needed to analyze thoroughly the temperature profiles in the spirally wound cells and to refine the modeling.

#### *Thermal runaway simulation:*

Explosive failures are often associated with localized temperatures above the melting point of Li (2, 3). Therefore, initiation of thermal runaway was simulated by assuming that a hot spot, located near the center of the cell, is formed via a localized exothermic chemical reaction (for example, between Li and sulfur or a sulfur compound) or cell defect. Two simulations were run with the hot spot located at two different points in the cell. For case one, the hot spot was located at the center of the cell in the separator region bordering the cathode and electrolyte. For case two, the hot spot was located in the center of the electrolyte in the middle of the spiral. Case two was also approximated using the one-dimensional circles model for comparison purposes. The hot spot areas were approximately  $0.031 \text{ mm}^2$

and  $0.029 \text{ mm}^2$  for case one and two, respectively. The finite element meshes were refined until results were accurate to within 1 K for case one and 3.5 K for case two.

The conditions under which thermal runaway usually occur include high discharge rates and high temperatures (2, 3-5). Therefore, the inputs to the model included an environmental temperature of 390 K, a uniform initial temperature in the cell of 390 K, and a uniform heat generation rate of  $1 \times 10^5 \text{ W/cm}^3$ . The hot spot heat generation rate,  $\dot{q}_d'''$ , was set equal to  $5 \times 10^8 \text{ W/cm}^3$ . The simulations were run until the minimum temperature in the cell exceeded the melting point of Li (453.6 K). It was assumed that when temperatures exceed the melting point of Li, molten Li bridges the gap between anode and cathode, forming an internal short circuit. Upon forming the short, it was assumed that  $\dot{q}_d'''$  would become infinitely large, the temperature would soar, and in a matter of milliseconds the cell would vent or explode (11).

Figure 10 shows the maximum and minimum temperature-time curves for case one, case two, and the circles approximation to case two. The maximum temperature increases much more rapidly in case 2 than in case 1. In case 2, the hot spot is isolated from the more conductive regions of the cell by the electrolyte. In case 1, the hot spot borders the cathode region and the heat is better conducted out the cell via the spiral path. Note that the spiral geometry still improves the heat transfer in case 2 as is indicated by the higher temperatures predicted using the circles model.

Figure 11 shows a two-dimensional temperature profile for case two approximately 470 seconds after initiation of the hot spot, corresponding to the box in Fig. 10. A temperature spike is located in the electrolyte region where the hot spot is centered. Note that minimum temperatures exist around most of the cell perimeter except for a portion of the cell located near the end of the spiral (i.e., between points A and B in Fig. 3). This rise in temperature at the spiral end is

due to the insulated boundary conditions applied at this boundary. In the actual cell (Fig. 1) the end of the spiral borders electrolyte (or cell gases if the electrolyte has been used up) and one would expect heat flow to be inhibited at this juncture. This result indicates that it is important how the end of the spiral is treated in the actual design. If possible, the end of the spiral should be in close proximity to the case can and void space should be minimized. Researchers (3) have observed that the temperature distribution over the exterior wall of the cell varies, some regions at high temperatures relative to the rest of the exterior surface. Perhaps these high temperature areas correspond to the location of the spiral end in the cell interior.

Many situations, both normal operation and thermal runaway conditions, can be simulated using the model. These simulations can lead to a better understanding of the thermal behavior of this design as has been achieved here. Indeed the power of the model lies in the ability to investigate various scenarios simply by changing model inputs. The modeling can also be used as an aid in the interpretation of experimental data, as has been done here.

## CONCLUSIONS

A two-dimensional thermal model of a spirally wound  $\text{Li}/\text{SOCl}_2$  cell has been developed. The model and two one-dimensional approximations have been used to understand better the thermal behavior of this battery. Comparison of model predictions with experimental data support two contentions. The heat generation rate seems to be greatest at the center of the cell and diminishes towards the exterior of the cell. Also, thermal conductivities seem to decrease as the cell discharges. This could be due to the increasing volume occupied by cell gases as the discharge proceeds. Two thermal runaway situations were investigated using the model based on the theory that localized hot spots initiate thermal runaway. The effectiveness of the spiral design in conducting heat out of the cell is dependent upon where these hot spots are located in the cell. If hot spots are in contact with those regions of the cell having relatively high thermal conductivities then the spiral design serves to improve significantly heat dissipation.

The model could be modified to investigate other physical situations. For example, forced convection, radiation, and conduction (via a potting material, e.g.) at the cell boundaries could be included in the boundary conditions of the model. Also, the model could be applied to other spirally wound batteries simply by changing model inputs (e.g., thermal conductivities, thermoneutral potential). Improvements to the model might include extending the model to three dimensions using the computer code TOPAZ3D (37), including contact resistances between regions, and adding temperature dependent thermophysical properties (10).

## ACKNOWLEDGEMENT

The authors acknowledge gratefully the National Aeronautics and Space Administration for their funding of this work under Grant No. NAG. 9-177. Also, the authors wish to thank Eric Darcy and Bob Bragg at the National Aeronautics and Space Administration for their inputs to this work, Art Shapiro at the Lawrence Livermore National Laboratory for his help in debugging input files to TOPAZ2D, the professionals at the Jet Propulsion Laboratory for their suggestions for the modeling, and the Cray Research Center, Inc., in Houston, TX for use of their CRAY. Special thanks to Bill Eue at the Cray Research Center for his help in converting some of the program code.

## LIST OF SYMBOLS

$c_{p,k}$	specific heat of material $k$ , J/Kg-K
$E$	cell voltage, V
$E_{oc}$	open-circuit voltage of the cell, V
$E_{tn}$	thermoneutral potential of the cell, V
$F$	Faraday's constant, 96487 C/mol of electrons
$h$	heat transfer coefficient, W/m <sup>2</sup> K
$I$	total cell current, A
$n_x$	normal vector in the $x$ direction
$n_y$	normal vector in the $y$ direction
$p_k$	property of material $k$
$\bar{p}$	average property of core region
$\dot{q}_j'''$	heat generation rate due to source $j$ , W/m <sup>3</sup>
$\dot{q}_p'''$	heat generated due to cell polarization, W/m <sup>3</sup>
$\dot{q}_s'''$	heat generated due to entropy effects, W/m <sup>3</sup>
$t$	time, s
$T$	cell temperature, K
$T_A$	ambient temperature, K
$V_{cell}$	cell volume, m <sup>3</sup>
$x$	dimension defining two-dimensional plane, m
$y$	dimension defining two-dimensional plane, m

### Greek Symbols

$\delta_k$	thickness of region $k$ , m
$\epsilon$	porosity or void volume fraction
$\lambda_k$	thermal conductivity of region $k$ , W/m-K
$\rho_k$	density of material $k$ , Kg/m <sup>3</sup>

### Subscripts

$A$	ambient conditions
$k$	region $k$
$j$	source $j$ (either $p$ , $s$ , or $d$ )
$oc$	open circuit
$w$	conditions at the wall
$x$	$x$ dimension
$y$	$y$ dimension

## REFERENCES

1. D. H. Johnson, A. D. Ayers, R. L. Zupancic, V. S. Alberto, and J. C. Bailey, *J. Power Sources*, **12**, 61 (1984).
2. S. Surampudi, G. Halpert, and I. Stein, "Safety Considerations of Lithium-Thionyl Chloride Cells," JPL publication 86-15 (June 1986).
3. J. B. Trout, "Studies of Performance and Abuse Resistance of Lithium-Bromine Complex Cells for Manned Space Use," NASA internal note JSC-20006, July 1984.
4. N. C. Luksa, "Li-BCX D-Cell Overdischarge," NASA internal note JSC-19262, October 1983.
5. D. Saucier, "Lithium BCX Cell Overdischarge Test," NASA internal note JSC-19548, April 1984.
6. K. M. Abraham, L. Pitts, and W. P. Kilroy, *J. Electrochem. Soc.*, **132**, 2301 (1985).
7. S. Szpak and H. V. Venkatesetty, *Power Sources 9: Research and Development in Non-Mechanical Electrical Power Sources*, Proceedings of the 13th International Power Sources Symposium held at Brighton, Sept. 1982, J. Thompson, Ed., Academic Press, London, England, 403 (1983).
8. D. Bernardi, E. Pawlikowski, and J. Newman, *J. Electrochem. Soc.*, **132**, 5 (1985).
9. J. Lee, K. W. Choi, N. P. Yao, and C. C. Christianson, *J. Electrochem. Soc.*, **133**, 1286 (1986).
10. L. A. Parnell and S. Szpak, *Electrochimica Acta*, **30**, 913 (1985).
11. S. Szpak, C. J. Gabriel, and J. R. Driscoll, *Electrochimica Acta*, **32**, 239 (1987).
12. Y. I. Cho and G. Halpert, "Heat Dissipation of High Rate Li-SOCl<sub>2</sub> Primary Cells," *J. Power Sources* (1986).
13. T. I. Evans, T. V. Nguyen, and R. E. White, submitted for publication to the *J. Electrochem. Soc.*
14. K. C. Tsaur and R. Pollard, *J. Electrochem. Soc.*, **131**, 975 (1984).
15. K. C. Tsaur and R. Pollard, *J. Electrochem. Soc.*, **131**, 984 (1984).
16. K. C. Tsaur, "Analysis of Electrochemical Systems with Multiple Reactions," Ph.D. dissertation, University of Houston, Houston, TX, (1984).
17. K. C. Tsaur and R. Pollard, *J. Electrochem. Soc.*, **133**, 2296 (1986).
18. Y. I. Cho and G. Halpert, "Thermal Analysis of Prismatic Li-SOCl<sub>2</sub> Primary Cells," presented at the 32<sup>nd</sup> International Power Series Symposium, Cherry Hill, NJ (May, 1986).

19. Y. I. Cho, *J. Electrochem. Soc.*, **134**, 771 (1987).
20. J. Newman and W. Tiedemann, *AIChE. J.*, **21**, 25 (1975).
21. J. A. Trainham, "Flow-Through Porous Electrodes," Ph.D. Dissertation, University of California, Berkeley, CA, (1979).
22. K. Nisancioglu, "Diffusion in Concentrated Electrolyte Solutions," M.S. Thesis, University of California, Berkeley, CA, (1970).
23. J. Newman, D. Bennion, and C. W. Tobias, *Ber. Bunsenges. Phys. Chem.*, **69**, 608 (1965).
24. J. S. Newman, "Electrochemical Systems," Prentice Hall, Inc., Englewood Cliffs, NJ (1973).
25. K. A. Klinedinst, *J. Electrochem. Soc.*, **132**, 2044 (1985).
26. N. A. Godshall and J. R. Driscoll, *J. Electrochem. Soc.*, **131**, 2221 (1984).
27. L. D. Hansen and H. Frank, *J. Electrochem. Soc.*, **134**, 1 (1987).
28. L. Lapidus and G. F. Pinder, "Numerical Solution of Partial Differential Equations in Science and Engineering," John Wiley & Sons, Inc., New York, NY (1982).
29. A. B. Shapiro, "TOPAZ2D - A Two-Dimensional Finite Element Code for Heat Transfer Analysis, Electrostatic, and Magnetostatic Problems," Lawrence Livermore National Laboratory, UCID-20824 (July 1986).
30. J. O. Hallquist, "MAZE - An Input Generator for DYNA2D and NIKE2D," Lawrence Livermore National Laboratory, UCID-19029, Rev. 2 (June 1983).
31. Wilson-Greatbatch, personal communications.
32. B. Bragg and E. Darcy, National Aeronautics and Space Administration, personal communications.
33. W. K. Behl, J. A. Christopoulos, M. Ramirez, and S. Gilman, *J. Electrochem. Soc.*, **120**, 1619 (1973).
34. J. J. Auborn, K. W. French, S. I. Lieberman, V. K. Shah, and A. Heller, *J. Electrochem. Soc.*, **120**, 1613 (1973).
35. K. A. Klinedinst and M. J. Domeniconi, *J. Electrochem. Soc.*, **127**, 539 (1980).
36. A. N. Dey, *J. Electrochem. Soc.*, **126**, 2052 (1979).
37. A. B. Shapiro, "TOPAZ3D - A Three-Dimensional Finite Element Heat Transfer Code," Lawrence Livermore National Laboratory, UCID-20484 (August 1985).
38. G. Halpert, Jet Propulsion Laboratory, personal communications.
39. J. A. Dean, "Lange's Handbook of Chemistry," 13<sup>th</sup> ed., McGraw Hill Book Co., Inc., New York, NY (1985).

Table I. Cell specifications for a spirally wound Li/SOCl<sub>2</sub> cell

Cell specification	Value	References
Thickness of cathode	1.12 mm	31, 38
Porosity of cathode	0.85	10, 38
Thickness of anode	0.7 mm	31, 32, 38
Thickness of current collector	0.14 mm	31, 32, 38
Thickness of separator	0.14 mm	31, 32, 38
Porosity of separator	0.7	38
Number of wraps	$\approx 3 \frac{1}{2}$	31, 32
D-size cell volume	$\approx 4.94 \times 10^4 \text{ mm}^3$	31, 32

Table II. Model inputs

<u>Thermophysical properties</u>				
Material	Density (Kg/m <sup>3</sup> )	Thermal conductivity (W/m-K)	Specific heat (J 'Kg-K)	References
Lithium anode	534.0	71.1	3490.0	10, 11, 39
Nickel current collector	8900.0	90.5	444.0	11, 19
Carbon	1950.0	23.8	712.0	10, 11
Glass matting	220.0	0.242	963.0	10, 11, 38
Electrolyte (1.8M LiAlCl <sub>4</sub> in SOCl <sub>2</sub> )	1690.0	0.143	1000.0	11, 19, 38
Cathode region	1730.0	3.69	957.0	10, 11, 19, 38
Separator region	1250.0	0.173	989.0	10, 11, 38
Core region	1755.0	23.82	1577.0	see Eq. [8]
<u>Model parameters</u>				
Parameter	References			
$h = 10 \text{ W/m}^2\text{-K}$	11, 13, 14			
$E_{tn} = 3.723 \text{ V}$	26			

Table III. Thermophysical properties of porous regions assuming that the voids are filled with SO<sub>2</sub> at approximately 20 psig and 60 °C

Material	Density (Kg/m <sup>3</sup> )	Thermal conductivity (W/m-K)	Specific heat (J/Kg-K)	References
SO <sub>2</sub>	5.54	0.00816	654.0	39
Cathode region	298.0	3.577	662.0	
Separator region	70.0	0.0783	746.3	

## LIST OF FIGURE CAPTIONS

- Fig. 1 Schematic representation of a spirally wound battery.
- Fig. 2 Top view of a spirally wound battery.
- Fig. 3 The two-dimensional model region for the spiral design.
- Fig. 4 One-dimensional approximations to the spiral design. The top schematic is the concentric circles approximation and the bottom schematic is the core region approximation.
- Fig. 5 Temperature-time curves predicted using the core, circles, and spiral models.
- Fig. 6 Heat generation rate and cell voltage for a 4 A discharge.
- Fig. 7 Predicted temperature profile after 1.5 hr of discharge.
- Fig. 8 Radial temperature profiles as predicted using the core, circles, and spiral models.
- Fig. 9 Comparison of predicted and experimental temperature-time curves for a 4 A discharge of a C-size Li/SOCl<sub>2</sub> cell.
- Fig. 10 Temperature-time curves for two thermal runaway cases.
- Fig. 11 Temperature profile in spirally wound Li/SOCl<sub>2</sub> cell for thermal runaway case two approximately 470 s after hot spot initiation. Internal temperatures exceed the melting point of Lithium.

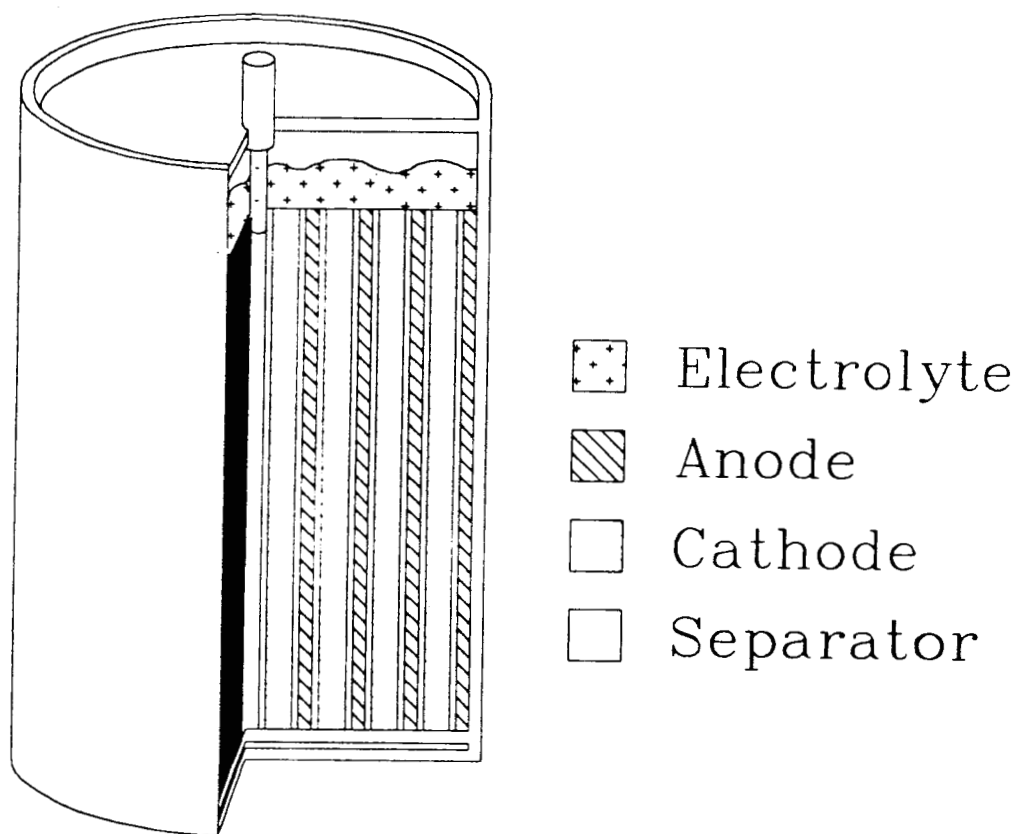
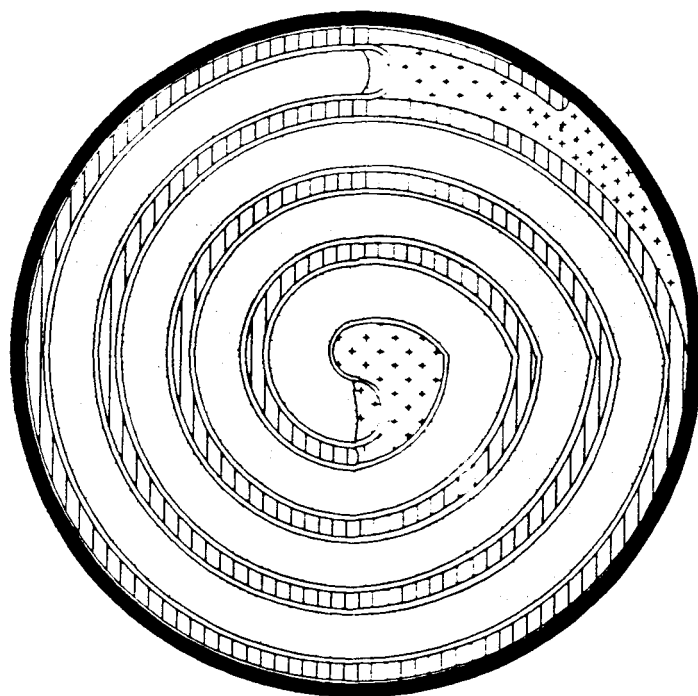





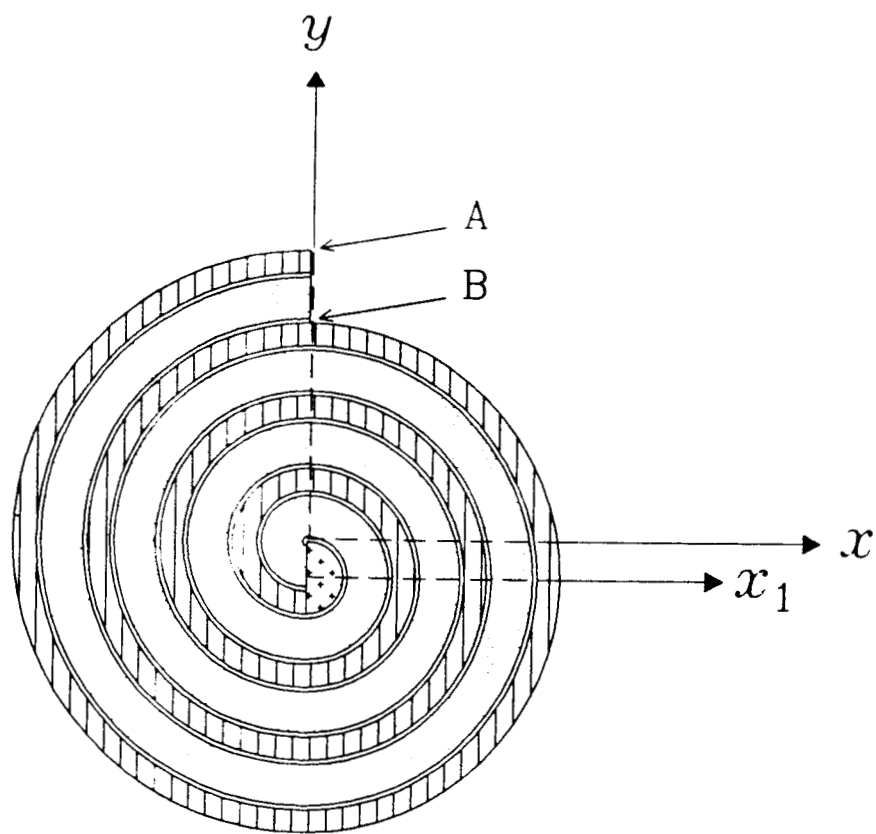


Fig. 1 Evans and White



-  Electrolyte
-  Anode
-  Cathode
-  Separator
-  Case

*Fig. 2 Evans and White*







-  Electrolyte
-  Anode
-  Cathode
-  Separator

Fig 3 Enns and White

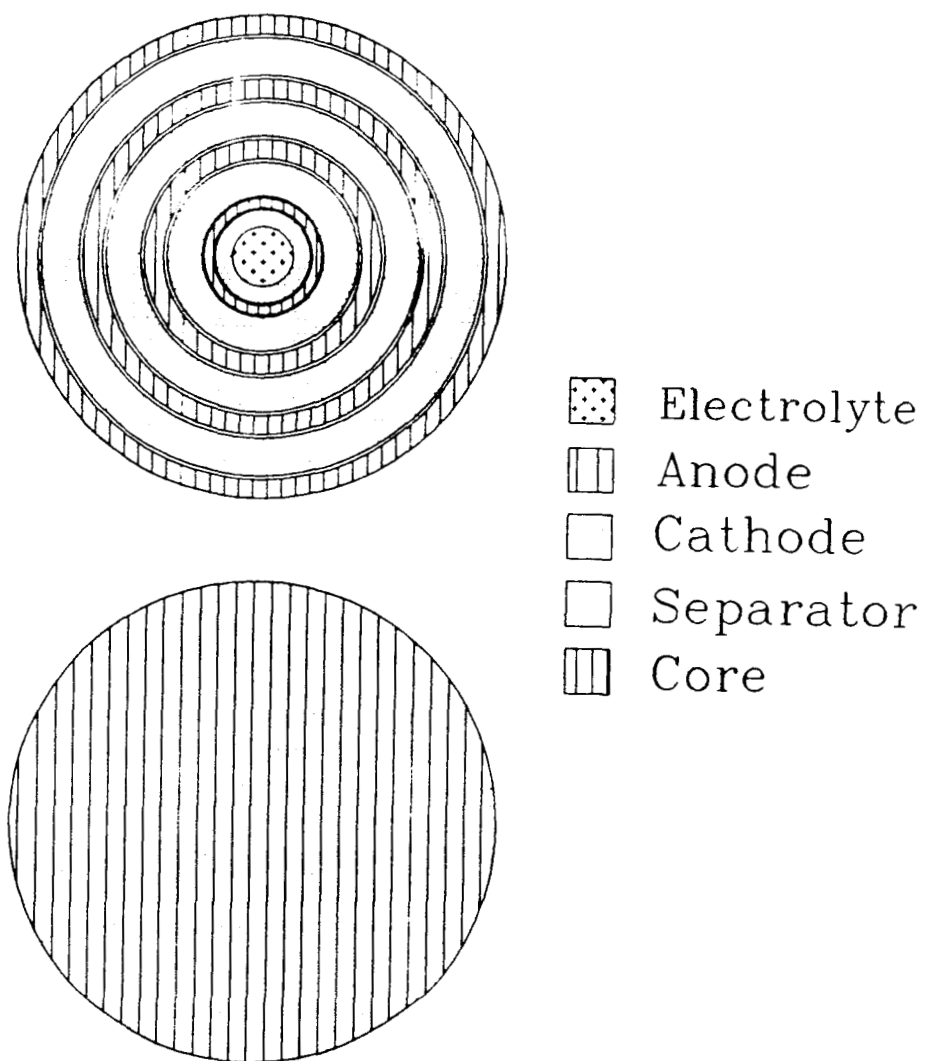


Fig 4 Evans and White

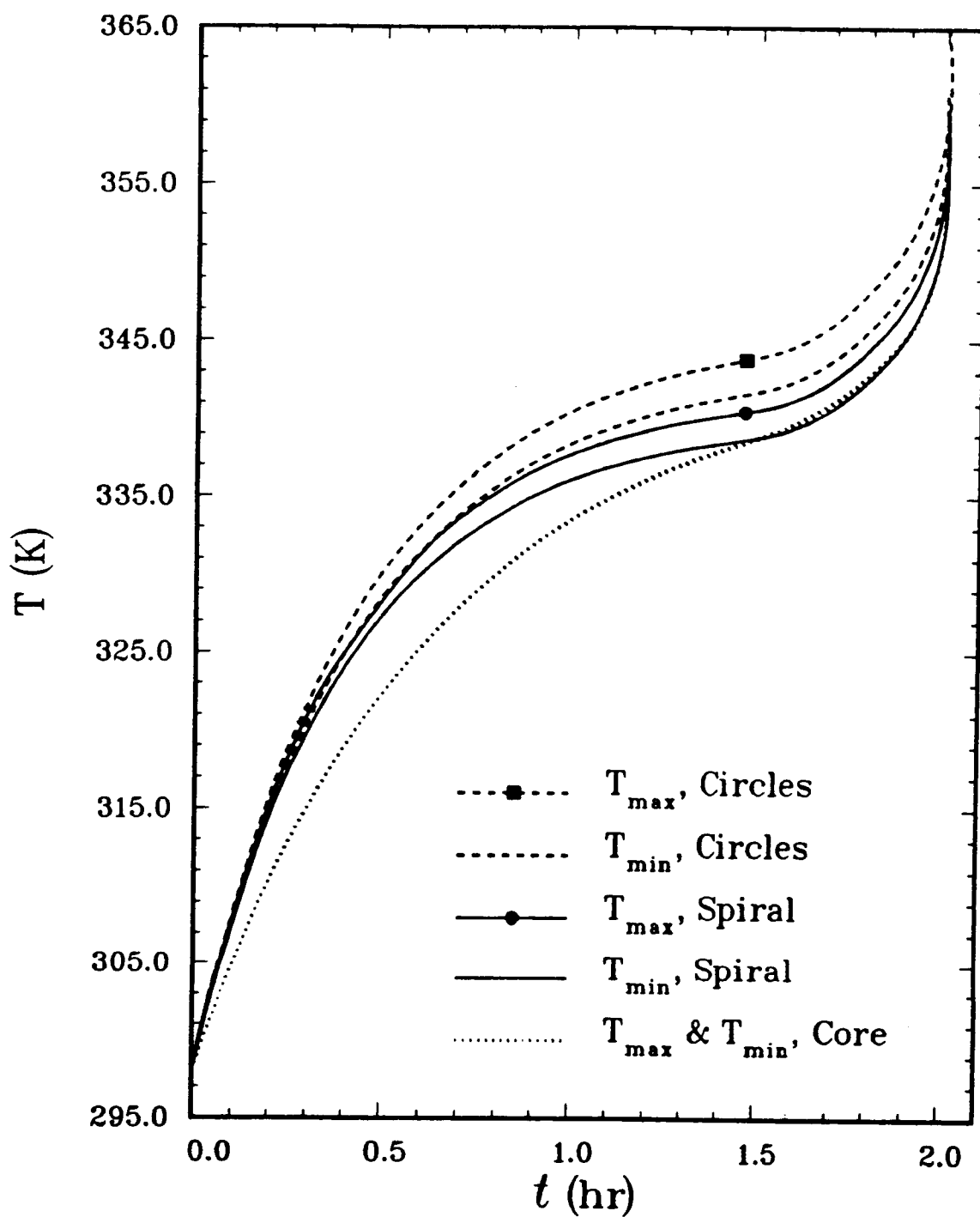


Fig 5 Evans and White

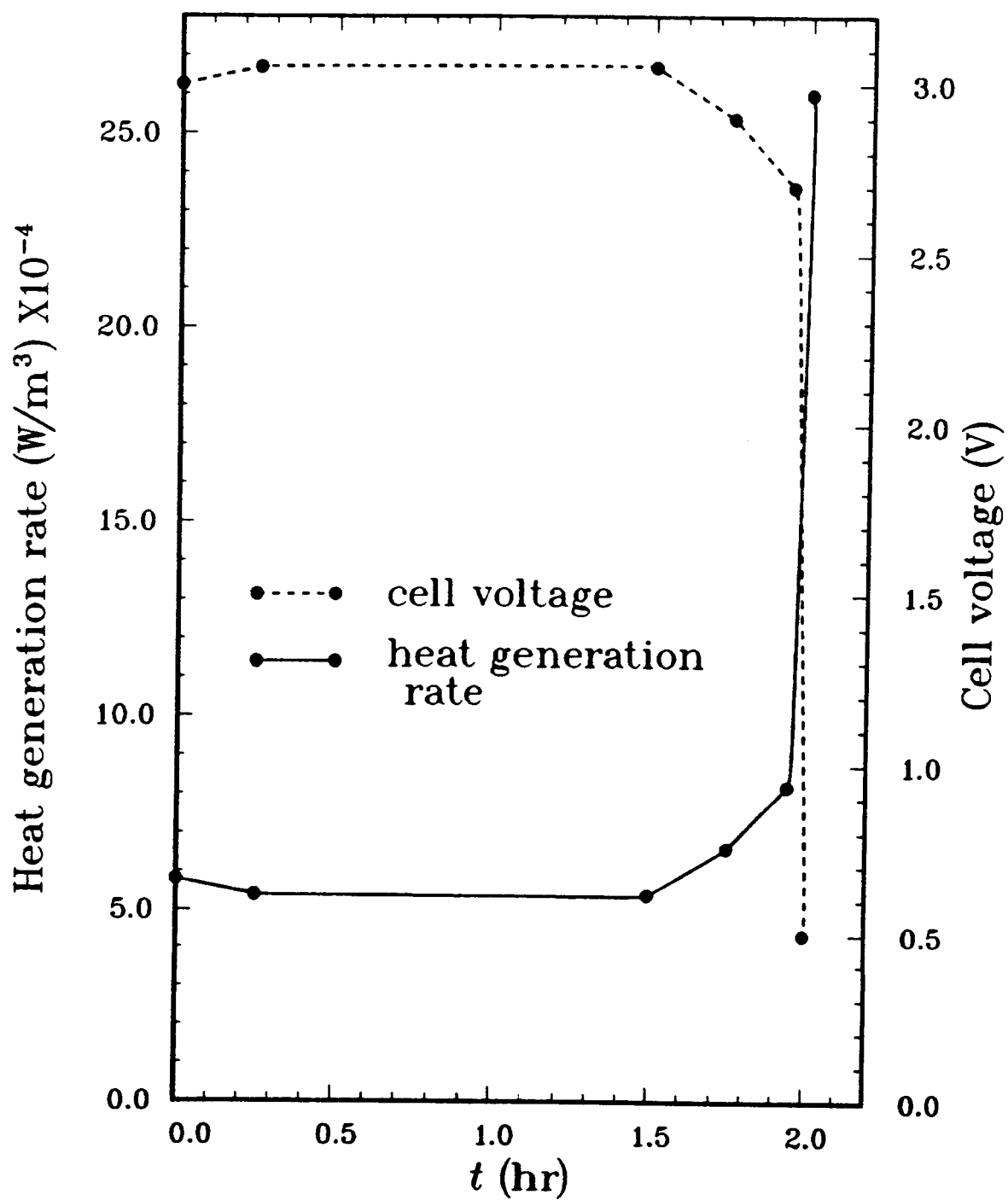


Fig. 6 Evans and White

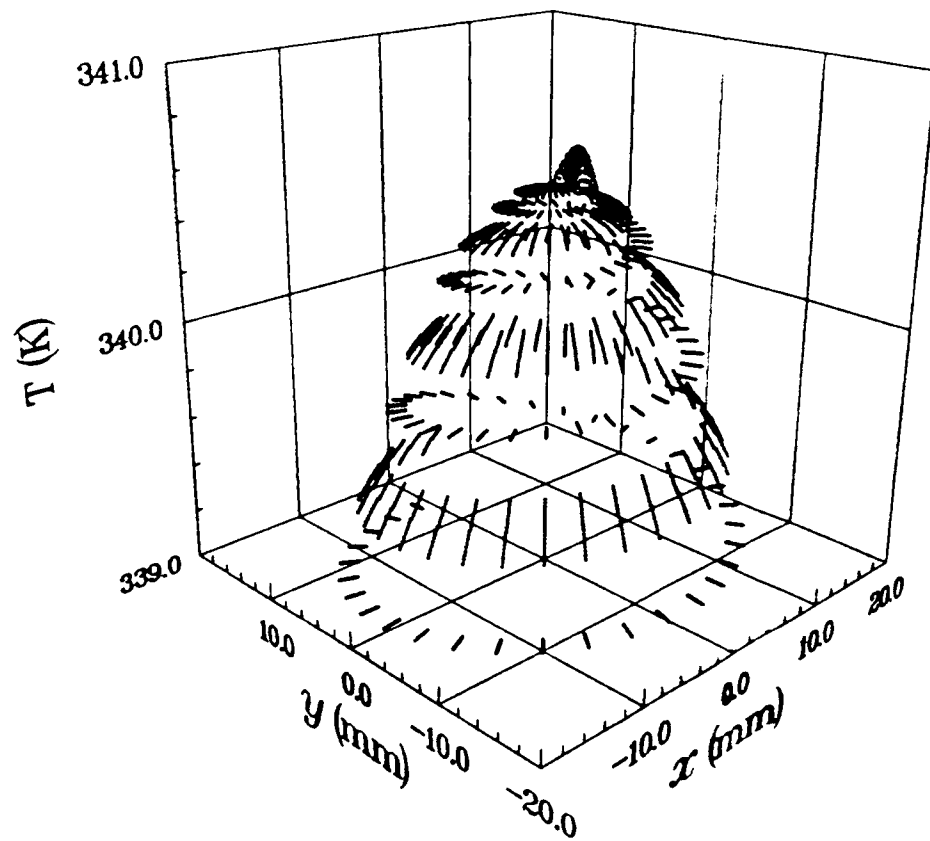


Fig 7 Erase and white

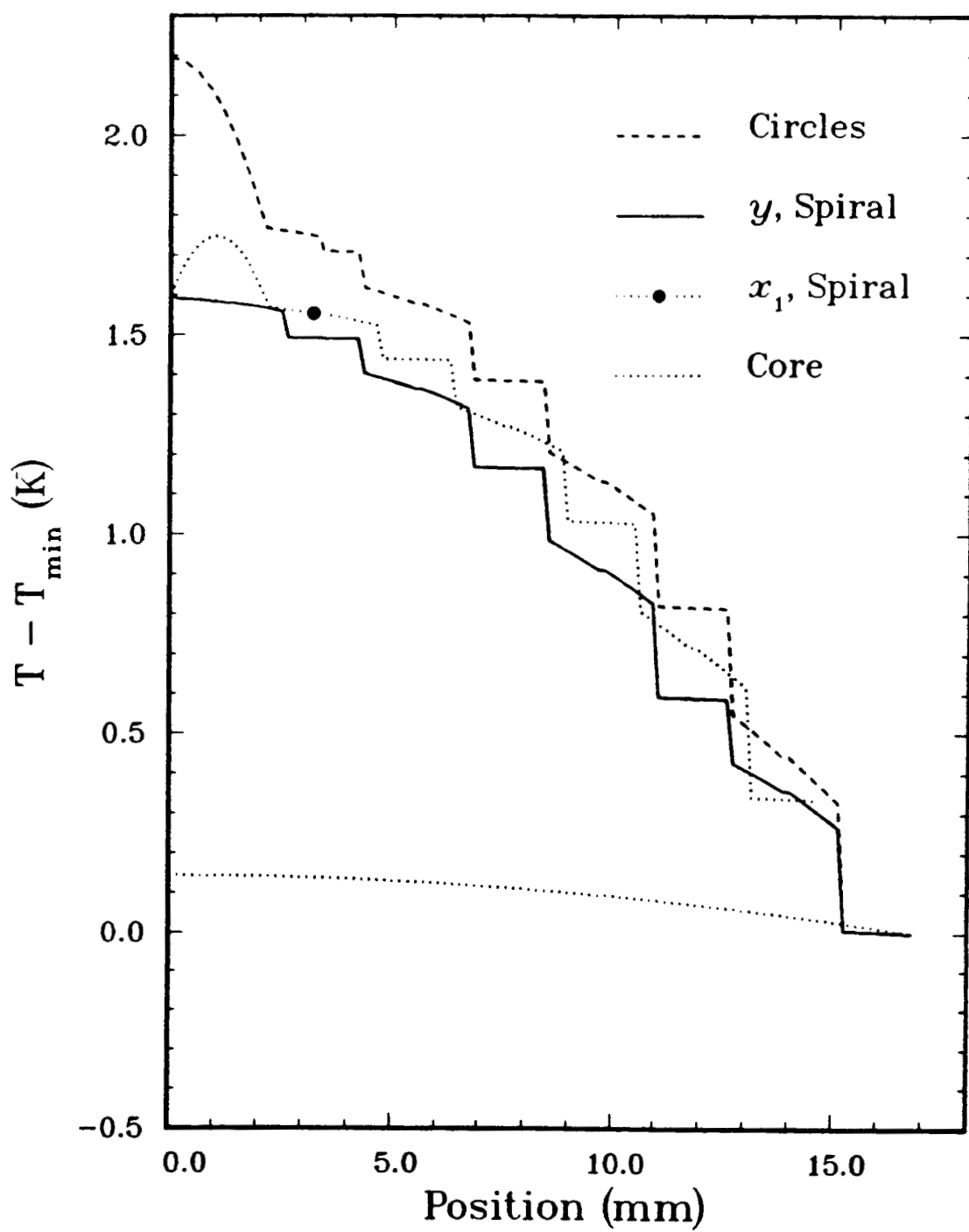


Fig. 8 Erane and White

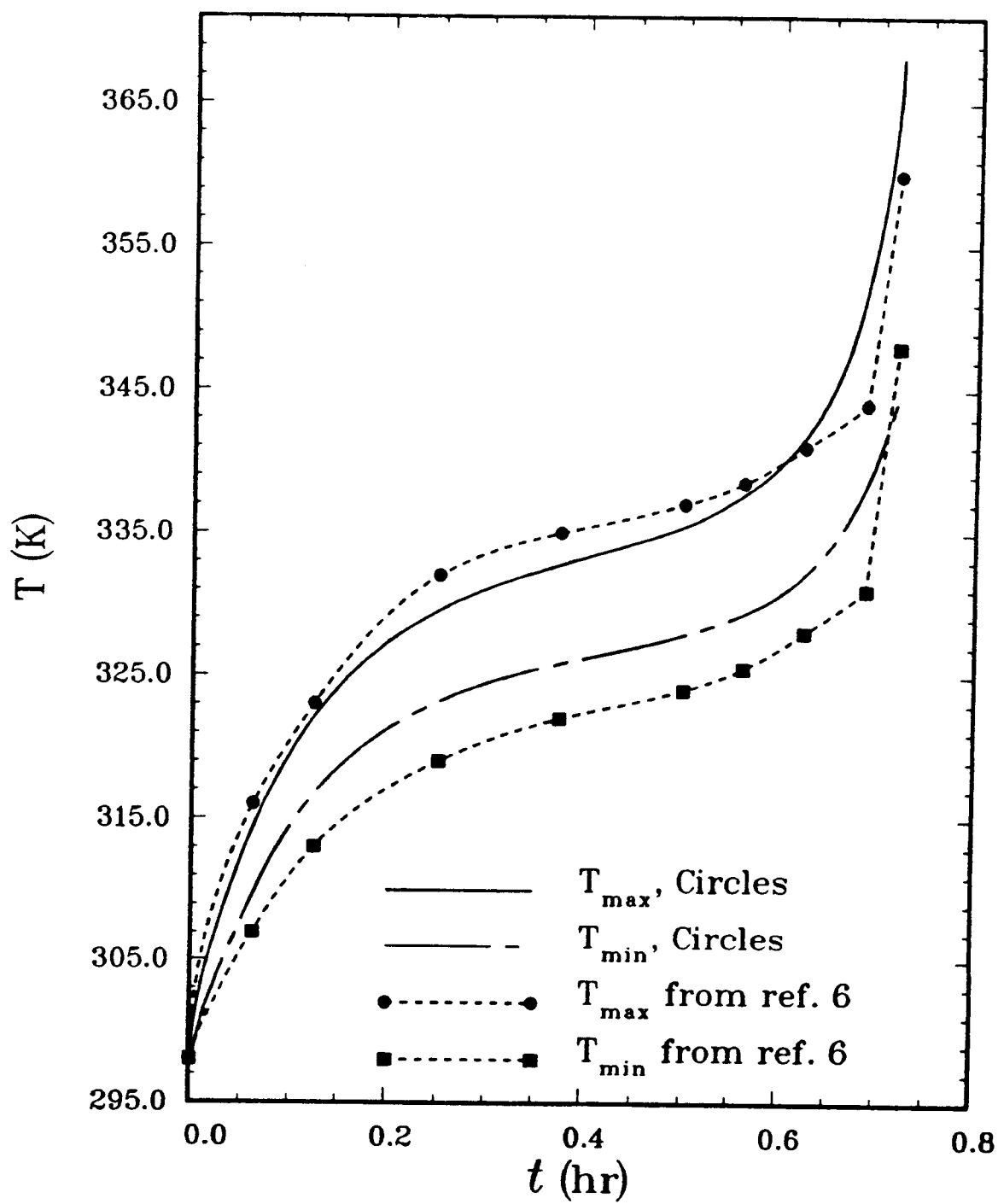


Fig. 9 Evans and White

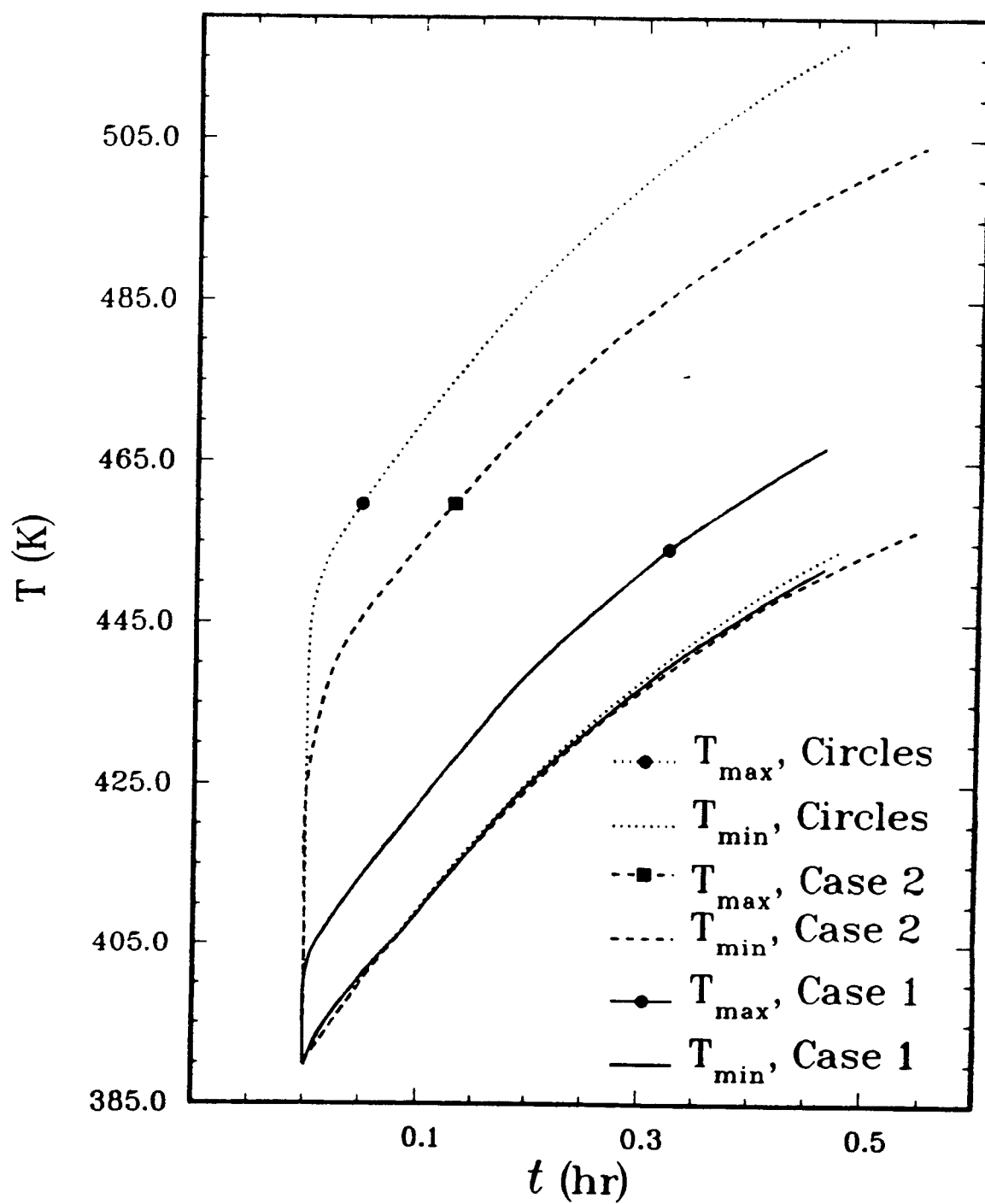


Fig. 10 Evans and White

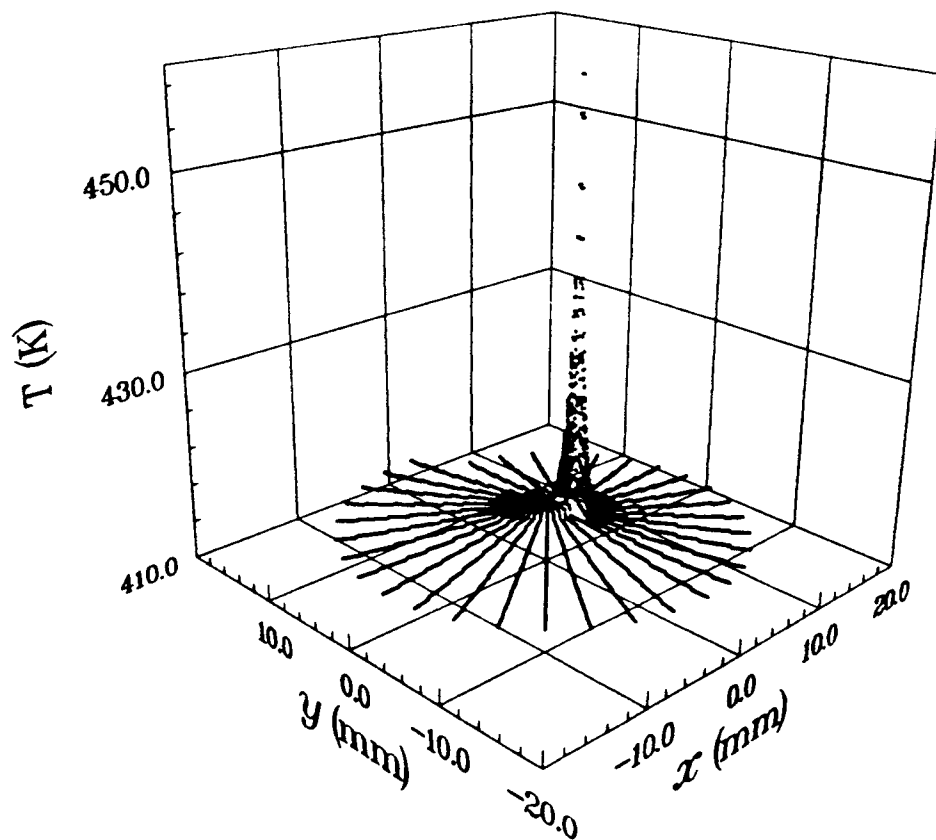


Fig. 11 Evans and White